

The impact of spatiotemporal structure of rainfall on flood frequency over a small urban watershed: an approach coupling stochastic storm transposition and hydrologic modeling

Zhengzheng Zhou¹, James A. Smith², Mary Lynn Baeck², Daniel B. Wright³, Brianne K. Smith⁴, Shuguang Liu¹

¹Department of Hydraulic Engineering, Tongji University, Shanghai, China.

²Department of Civil and Environmental Engineering, Princeton University, USA.

³Department of Civil and Environmental Engineering, University of Wisconsin-Madison, USA.

⁴Department of Earth and Environmental Sciences, City University of New York-Brooklyn College, USA.

Corresponding to: Zhengzheng Zhou (zhouzz@tongji.edu.cn); Shuguang Liu (liusgliu@tongji.edu.cn)

Abstract. The role of rainfall space-time structure, as well as its complex interactions with land surface properties, in flood response remains an open research issue. This study contributes to this understanding, specifically in small (<15 km²) urban watersheds. Using a flood frequency analysis framework that combines stochastic storm transposition-based (SST) rainfall scenarios with the physically-based distributed GSSHA model, we examine the role of rainfall spatial and temporal variability in flood frequency across drainage scales in the highly-urbanized Dead Run watershed (14.3 km²)-~~outside of Baltimore~~, Maryland, USA. The results show the complexities of flood response within several subwatersheds for both short (<50 years) and long (>100 years) rainfall return periods. The impact of impervious area on flood response decreases with increasing rainfall return period. For extreme storms, the maximum discharge is closely linked to the spatial structure of rainfall, especially storm core spatial coverage. The spatial heterogeneity of rainfall increases flood peak magnitudes by 50% on average at the watershed outlet and its subwatersheds for both small and large return periods. The framework of SST-GSSHA-coupled frequency analysis also highlights ~~results imply that commonly made assumption of spatially-uniform distributed rainfall scenarios are needed in urban-quick-response flood frequency modeling is problematic~~ even for relatively small basin scales.

1. Introduction

Rainfall spatiotemporal structure plays an important role in flood generation in urban watersheds (Saghafian *et al.*, 1995; Smith *et al.*, 2005b; Emmanuel *et al.*, 2012; Nikolopoulos *et al.*, 2014). Spatial heterogeneities in land use and land cover complicate the translation of rainfall spatiotemporal distribution into flood responses (Galster *et al.*, 2006; Morin *et al.*, 2006; Ntelekos *et al.*, 2008; Ogden *et al.*, 2011; Yin *et al.*, 2016; ten Veldhuis *et al.*, 2018), especially for small catchments (Faurès *et al.*, 1995; Smith *et al.*, 2005a; Zhou *et al.*, 2017; Zhou *et al.*, 2019; Yang *et al.*, 2020). ~~Due to the varying nature~~

~~of rainfall and complexities of urban characteristics,~~ The influence of rainfall spatial-temporal structure on flood frequency analysis in urban areas remains an open research issue.

~~Previous studies have demonstrated the sensitivity of hydrological response to rainfall variability in both space and time (Smith *et al.*, 2012; Ochoa-Rodriguez *et al.*, 2015; Rafiecinasab *et al.*, 2015). Many studies have examined the interaction between rainfall variability and flood response. By necessity, early studies tended to explore rainfall variability using rain gages, which were the main source of rainfall measurements until relatively recently. The accuracy of flood simulations using spatially detailed rainfall scenarios has been examined (Dawdy and Bergmann, 1969; Schilling, 1991), along with the sensitivity of hydrologic response to rainfall gage network density (Faurès *et al.*, 1995; Arnaud *et al.*, 2002; Younger *et al.*, 2009; Notaro *et al.*, 2013). Beven and Hornberger (1982) argued that the spatial variability affects the response time more than the peak magnitude, whereas Wilson *et al.* (1979) found the reverse. These studies were limited, however, by the general sparsity of rain gages, which may not adequately capture the spatial distribution of rainfall. Following the advent of rainfall measurement using weather radar (Fulton *et al.*, 1998; Krajewski and Smith, 2002), many studies have highlighted the use of high-resolution rainfall data in assessing rainfall variability over various range of spatial and temporal scales (Berne *et al.*, 2004; Gebremichael and Krajewski, 2004; Moreau *et al.*, 2009; Emmanuel *et al.*, 2012) and how their use could improve runoff estimation (Morin *et al.*, 2006; Smith *et al.*, 2007; Schellart *et al.*, 2012; Wright *et al.*, 2014b; Rafiecinasab *et al.*, 2015; Gourley *et al.*, 2017). {Wright, 2014 #230} {Wright, 2013 #4}~~

There are conflicting findings on the relative importance of rainfall temporal and spatial characteristics. Paschalis *et al.* (2014), Ochoa-Rodriguez *et al.* (2015) and Yang *et al.* (2016), ~~for example~~, found that “coarsening” temporal resolution has a stronger impact than coarsening spatial resolution, ~~especially for small watersheds. Similar results were found in the study of Paschalis *et al.* (2014) in a 477 km² catchment in Switzerland.~~ Adams *et al.* (2012) found the space-time averaging effects of routing through the catchment noticeably remove the impact of spatially variable rainfall at a 150-km² catchment scale. Bruni *et al.* (2015), in contrast, found a higher sensitivity of modeled flow peaks to spatial resolution rather than the temporal resolution. Peleg *et al.* (2017) showed an increasing contribution of the spatial variability of rainfall to the variability of flow discharge with longer return periods. Cristiano *et al.* (2018); Cristiano *et al.* (2019) found the spatial aggregation of rainfall data can have a strong effect on hydrological responses. Zhu *et al.* (2018) examined the influence of rainfall variability on flood frequency analysis and addressed the impact of antecedent moisture in flood generation for various basin scales ~~ranging from 16 km² up to 4,400 km². Using observational data, Zhou *et al.* (2017) showed that the impact of antecedent moisture is low in a highly urbanized catchment.~~

~~Previous studies have demonstrated the sensitivity of hydrological response to rainfall variability in both space and time~~

60 ~~(Smith *et al.*, 2012; Ochoa Rodriguez *et al.*, 2015; Rafiecinasab *et al.*, 2015). The relationship between rainfall and flood~~
61 ~~are scale dependent, varying with rainfall patterns, basin characteristics, and runoff generation processes. However, there~~
62 ~~is still no clear answer on the relative importance of temporal and spatial features of rainfall on flood responses (Cristiano~~
63 ~~*et al.*, 2017). Moreover, studies focusing on small (< 15 km²) urbanized basins are relatively few (Peleg *et al.*, 2017) and~~
64 ~~the issues remain poorly understood.~~

65 Stochastic Storm Transposition (SST) was developed as a physically-based stochastic rainfall generator for rainfall
66 frequency analysis. Previous studies show that SST with relatively short-term rainfall records (10 or more years) of high-
67 resolution radar rainfall fields can produce reasonable rainfall scenarios with realistic spatial-temporal structure, which
68 cannot be provided by conventional design storm methods (Wright *et al.*, 2013; Wright *et al.*, 2017; Zhou *et al.*, 2019). In
69 the conventional approach, the idealized assumptions include idealized rainfall temporal structure, uniformed spatial
70 distribution and 1:1 rainfall-flood return periods equivalence (see (Wright *et al.*, 2013; Wright *et al.*, 2017; Zhou *et al.*,
71 2019), and references therein). These assumptions ignore the interaction between spatiotemporal structure of rainfall and
72 flood responses, which increases the uncertainty of frequency estimations. Coupled with hydrological models, the SST-
73 based framework can be used for multiscale rainfall frequency analysis and flood frequency analysis that accounts for
74 rainfall variability and surface characteristics (Wright *et al.*, 2014a; Perez *et al.*, 2019; Yu *et al.*, 2019; Wright *et al.*, 2020).
75 Previous studies have demonstrated the sensitivity of hydrological response to rainfall variability in both space and time
76 (Smith *et al.*, 2012; Ochoa Rodriguez *et al.*, 2015; Rafiecinasab *et al.*, 2015). The relationship between rainfall and flood
77 are scale-dependent, varying with rainfall patterns, basin characteristics, and runoff generation processes. However, there
78 is still no clear answer on the relative importance of temporal and spatial features of rainfall on flood responses (Cristiano
79 *et al.*, 2017). Moreover, studies focusing on small (<-15 km²) urbanized basins are relatively few (Peleg *et al.*, 2017) and
80 the issues remain poorly understood.

81
82 This study contributes to the understanding of the interaction between rainfall variability and flood response over small-
83 scale urbanized watersheds (<15 km²) for a short-duration rainfall and quick hydrologic response setting. We build on the
84 SST-based rainfall study of Zhou *et al.* (2019) using the physically-based hydrological model implementation introduced
85 by Smith *et al.* (2015) ~~in~~ for the Dead Run watershed outside of Baltimore, Maryland, USA. The framework of SST-based
86 rainfall frequency analysis coupled with a hydrological model provides an effective approach for detailed flood frequency
87 study (Wright *et al.*, 2014a; Yu *et al.*, 2019). Under the framework, we characterize the spatial and temporal features of
88 rainfall events under different return periods and examine their roles in determining flood frequency in small urban
89 watersheds. T-by-addressing the following questions will be addressed: (1) How does flood frequency in small urban

90 watersheds vary with diverse space-time rainfall structure and rainfall magnitude? (2) ~~Among the space-time feature of~~
91 ~~rainfall, w~~What are the dominant space-time feature of rainfall features that control flood peak distribution in small urban
92 watersheds? By answering the above questions, the study can improve the understanding of interactions between rainfall
93 and flood process in small urbanized area. In addition, some idealized assumption used in the convetional rainfall-flood
94 frequency analysis will be questioned.

95
96 ~~Using a framework that combines high-resolution realistic SST and radar-based rainfall scenarios with model-based flood~~
97 ~~frequency analysis, we characterize the spatial and temporal features of rainfall events under different return periods and~~
98 ~~examine their roles in determining flood frequency in small urban watersheds.~~The paper is organized as follows: in Section
99 2, we introduce the study region and describe the SST-based methodology, GSSHA model, and the metrics used to
100 characterize rainfall and flood response. In Section 3, we present model validation and analyses of flood frequency
101 distributions and rainfall-flood relationships. A summary and conclusions are presented in Section 4.

102 **2. Data and method**

103 **2.1 Study region and data**

104 The study focuses on the highly-urbanized 14.3 km² Dead Run (DR) watershed located west of Baltimore, Maryland, USA
105 (Fig. 1). DR is a tributary to the Gwynns Falls watershed, which is the principal study catchment of the Baltimore
106 Ecosystem Study (BES); ~~)-~~ Pickett and Cadenasso (2006). The basin has an impervious fraction of approximately 52.3%
107 (Table 1). The watershed has a dense network of six stream gauges with drainage areas ranging from 1.2 to 14.3 km² (Fig.
108 1; Table 1). The subwatersheds are developed after the implementation of the Maryland Stormwater Management Act of
109 1982 (Maryland, 1982) with many detention infrastructures such as small local ponds. The wealth of data for Dead Run
110 provides exceptional resources to examine rainfall and hydrologic response (Beighley and Moglen, 2002; Nelson *et al.*,
111 2006; Meierdiercks *et al.*, 2010; Smith *et al.*, 2015). For example, Meierdiercks *et al.* (2010) analyzed the impact of storm
112 drains and detention basins on a single storm event in DR, while Ogden *et al.* (2011) used the Gridded Surface Subsurface
113 Hydrologic Analysis (GSSHA) model to analyze the effects of storm drains, impervious area, and drainage density on
114 hydrologic response. Smith *et al.* (2015) created a DR model using GSSHA to examine the effects of storage and runoff
115 generation processes through analyses of a large number of storm events.

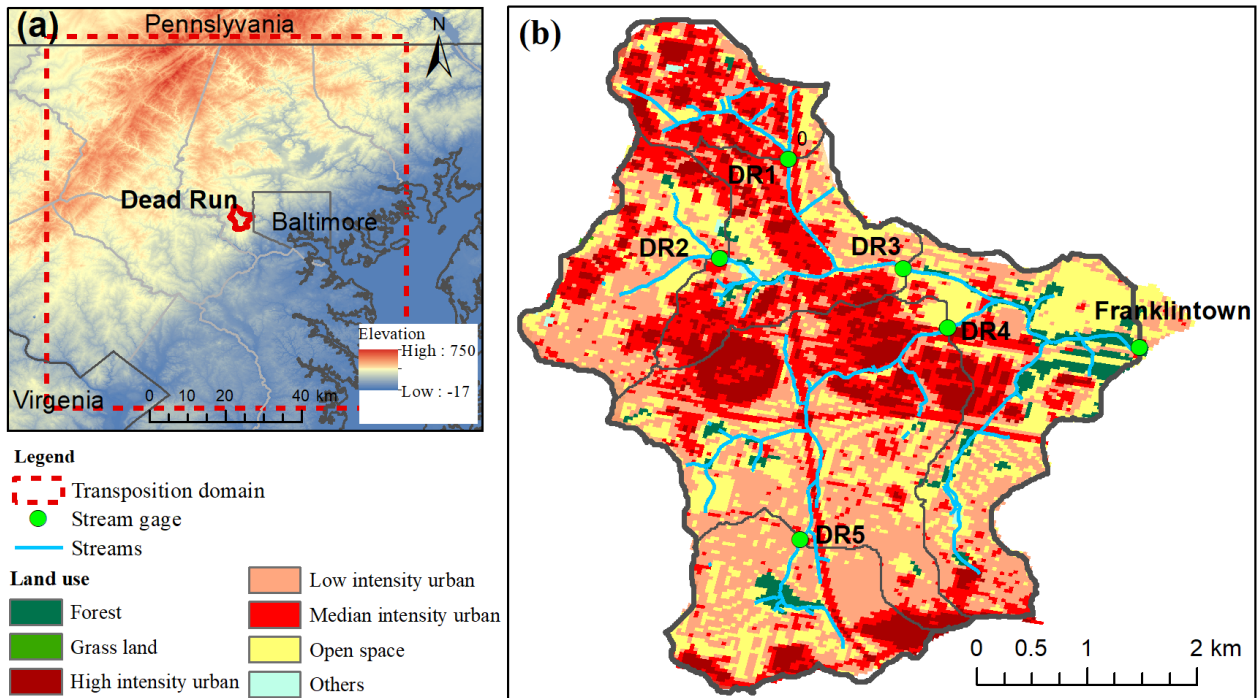


Figure 1. Overview of Dead Run study region including (a) location of DR, elevation, and transposition domain of SST; (b) land use land cover and stream gages. The red outline and grey outline in (a) indicates the boundary of DR watershed and Baltimore City, respectively.

High resolution (15-min temporal resolution, 1-km² spatial resolution) radar rainfall fields for the 2000-2015 period were derived from volume scan reflectivity fields from the Sterling, Virginia WSR-88D (Weather Surveillance Radar-1988 Doppler) radar. The two-dimensional radar rainfall fields are then developed from the reflectivity fields using the Hydro-NEXRAD algorithms (Krajewski *et al.*, 2011) which have been used in rainfall and hydrological studies (Smith *et al.*, 2007; Lin *et al.*, 2010; Smith *et al.*, 2013; Wright *et al.*, 2014b; Zhou *et al.*, 2017) are used to estimate rainfall from reflectivity fields. The Hydro-NEXRAD algorithms includes quality control algorithms, Z-R conversion of reflectivity to rainfall rate, time integration, and spatial mapping algorithms (Seo *et al.*, 2011). To improve the rainfall estimates, a multiplicative mean-field bias correction (Smith and Krajewski, 1991; Wright *et al.*, 2012) is applied on a daily basis using a network of 54 rain gauges in and around the Baltimore County. The bias computation takes the form $B_i = \frac{\sum_{S_i} G_{ij}}{\sum_{S_i} R_{ij}}$. Where G_{ij} is the rainfall accumulation for gage j on day i , R_{ij} is the daily rainfall accumulation for the co-located radar pixel accumulation on day i , and S_i is the index of the rain gage stations for which both the rain gage and the radar report positive rainfall accumulations for day i . Each 15-min radar rainfall field from day i is then multiplied by B_i . A network of 54 rain gauges in and around Baltimore City is used for mean field bias correction of the radar rainfall. The reader is directed to

135 Zhou *et al.* (2019) and references therein for further details on the rainfall data and bias correction methods.
 136 Instantaneous discharge data with a resolution of five minutes from the U.S. Geological Survey (USGS) were used for DR-
 137 1, DR-2, DR-5, and Franklinton ~~for each of the six gaged watersheds.~~ For DR-3 and DR-4, the discharge data is converted
 138 through stage discharge curves from (Lindner and Miller, 2012). Streamflow observations for the outlet station at
 139 Franklinton extend back to 1960. ~~T, while the DR1—DR5 subwatersheds stations~~ have records beginning in 2008.

140 **Table 1: Characteristics of Dead Run watershed** (Smith *et al.*, 2015).

	<u>USGS ID</u>	<u>Area</u> <u>(km²)</u>	<u>Developed Land^a</u> <u>(%)</u>	<u>Imperviousness</u> <u>(%)</u>	<u>Detention</u> <u>controlled</u> <u>area^b (%)</u>
<u>DR1</u>	<u>01589317</u>	<u>1.32</u>	<u>99%</u>	<u>73.6</u>	<u>41.9</u>
<u>DR2</u>	<u>01589316</u>	<u>1.92</u>	<u>98%</u>	<u>55.5</u>	<u>18.5</u>
<u>DR3</u>	<u>01589320</u>	<u>4.95</u>	<u>98%</u>	<u>62.2</u>	<u>24.4</u>
<u>DR4</u>	<u>01589315</u>	<u>6.29</u>	<u>98%</u>	<u>51.5</u>	<u>12.2</u>
<u>DR5</u>	<u>01589312</u>	<u>2.05</u>	<u>96%</u>	<u>47.9</u>	<u>3.2</u>
<u>Franklinton</u>	<u>01589330</u>	<u>14.3</u>	<u>96%</u>	<u>52.3</u>	<u>25.1</u>

Note:

a. Developed lands include “Developed, open space” (>20% impervious surface), “Developed, low intensity” (20%-49% impervious surface), “Developed, medium intensity” (50%-79% impervious surface), and “Developed, high intensity” (80% or more impervious surface). Data source: USGS 2012 National Land Cover Dataset (NLCD).

b. Detention controlled area^b refers to the area controlled by detention infrastructure.

141

142 **2.2 GSSHA Hydrological Model**

143 The distributed physics-based GSSHA model is used to simulate multi-scale flood response. GSSHA is a two-dimensional,
 144 distributed-parameter raster-based (i.e. square computational cell-based) hydrologic modeling system. It uses explicit finite
 145 difference and finite volume methods in two dimensions on a structured grid to simulate overland flow and in one dimension
 146 to simulate channel flow (Downer and Ogden, 2004; 2006). Previous studies of the GSSHA model show that the model
 147 with fine grid resolution can produce adequate simulations of flood response, especially when driven by high-resolution
 148 radar rainfall fields (Sharif *et al.*, 2010; Sharif *et al.*, 2013; Wright *et al.*, 2014a; Cristiano *et al.*, 2019).

149 In this study, we use the Dead Run model created by Smith *et al.* (2015). A brief description of the model is provided here;
 150 see Smith *et al.* (2015) for more details. The delineation of the watershed and channel network was based on a 30-m USGS
 151 digital elevation model (Gesch *et al.*, 2002). Channel flow overland flow was set with different Manning’s roughness
 152 coefficients. Additional stream channels were added based on the Baltimore County hydrography Geographic Information

153 Systems– (GIS) map. Stream cross sections were extracted from a 1-m resolution topography data set for Dead Run
154 developed from lidar. Storm sewers in DR-2 and DR-5 were added using the Baltimore County Stormwater Management
155 GIS map and digitized storm sewer maps. The semicircle’s diameter was set to the pipe diameter. Detention basins were
156 represented within the channel with cross sections extracted from the 1-m lidar topographic data.[3](#)
157 Several aspects of the model were modified from those used in Smith *et al.* (2015), primarily to improve computational
158 speed. Infiltration is calculated using Richards’ equation (RE) in Smith *et al.* (2015), while this study uses the three-layer
159 Green-Ampt (GA) scheme. A uniform Manning’s roughness coefficient of 0.01 is set for all the stream channels for model
160 simplification. Initial soil moisture is approximated to be one third of field capacity for each storm event.

161 **2.3 SST procedure**

162 The rainfall scenarios in this study are developed using RainyDay, an open-source SST software package (Wright *et al.*,
163 2017). The steps used are briefly summarized here; the reader is directed to Zhou *et al.* (2019) and references therein for
164 further details.

165 The first step is to identify a geospatial “transposition domain” that contains the watershed of interest. In this study, we use
166 a square 7,000 km² transposition domain centered on the DR watershed. (Zhou *et al.*, 2019) presented a detailed
167 examination of heterogeneity in extreme rainfall over the transposition domain using a variety of metrics, including storm
168 counts, mean storm depths and intensities, convective activity indicated by lightning observations, and analysis of spatial
169 and temporal rainfall structure.

170 The second step is to identify the largest m storms within the domain at the t -hr time scale. This collection of storms is
171 referred to as a storm catalog. The storms are selected with respect to the size, shape and orientation of the DR watershed.
172 We henceforth refer to these as “DR-shaped storms.” The m DR-shaped storms are selected from an n -year rainfall record,
173 such that an average of $\lambda=m/n$ storms per record year are included in the storm catalog. In this study, we chose $m = 200$
174 storms over the 16-year radar record.

175 The third step is to randomly sample a subset of k storms from the storm catalog, where k refers to a stochastic number of
176 storms per year. The k is assumed to follow a Poisson-distributed number of storm occurrences with rate parameter $\lambda=m/n$
177 storms per year. All rainfall fields associated with a storm are transposed by an east-west distance Δx and a north-south
178 distance Δy , where Δx and Δy are drawn from distributions $D_x(x)$ and $D_y(y)$ which are bounded by the limits of the
179 transposition domain. Based on the spatial heterogeneity analysis of extreme rainfall in the domain, distributions $D_x(x)$ and
180 $D_y(y)$ can be set as uniform or non-uniform. In Zhou *et al.* (2019) and this study, since the assumption of regional
181 homogeneity cannot be relaxed, we used the non-uniform distribution. A two-dimensional probability density function

(PDF) of spatial storm occurrence (Wright *et al.*, 2017) ~~and an intensity factor that rescales the rainfall magnitude (Zhou *et al.*, 2019) are is~~ used as the basis for non-uniform spatial transposition (Fig. A1 in Appendix A). This step can be understood as generating a “synthetic year” of extreme rainfall events over the domain based on resampling and transposing observations. For each of the k transposed storms, compute the t -hr basin-average rainfall depth over the watershed. Among the k rainfall depths, the maximum depth is retained as a synthetic t -hr annual rainfall maximum for the watershed, while the transposed rainfall fields are saved for use as inputs to a GSSHA model simulation.

The fourth step ~~simply~~ repeats Step 3 ~~many~~ S times to recreate multiple years of synthetic t -hour “annual” rainfall maxima and associated transposed rainfall fields for the watershed. In this study, these steps are repeated $S=31,000$ times and the ordered “annual” maxima are used to generate rainfall return period estimates up to 2500 years. 31,000 such realizations of 2500-yr series are generated, and the median value of 1,0300 realizations are used to generate estimates for return periods up to 2500 years.

2.4 Characteristics of rainfall and hydrologic response

2.4.1 Spatio-temporal characteristics of rainfall

Rainfall statistics were computed for each event, based on radar rainfall data at 15-min, 1-km² resolution, to characterize the spatial and temporal variability of rainfall (following Smith *et al.* (2002); Smith *et al.* (2005b); see also Zoccatelli *et al.* (2011) and Emmanuel *et al.* (2015)). ~~For basin scale of A, B~~ the basin-average rainfall rate (mm/h) at time t during the storm is given by:

$$M(t) = \int_{\theta A}^T R(t, x) dx \quad (1)$$

where $R(t, x)$ is the rain rate at radar grid x at time t , and T is the time period of rainfall event. Peak basin-average rainfall rate (mm/h) is denoted:

$$M_{max} = \max\{M(t); t \in [0, T]\} \quad (2)$$

and storm total rainfall depth (mm) is:

$$R_{sum} = \sum_0^T M(t) \quad (3)$$

To characterize the spatial properties of rainfall, several dimensionless quantities are computed. Fractional coverage of storm core at t is given by:

$$Z(t) = \frac{1}{A} \int_A I_{(R(t,x))} dx \quad (4)$$

208 where $I_{(R(t,x))}$ is the indicator function and equals 1 when $R(t, x) > 25 \text{ mm/h}$ or 0 otherwise.

209 Rainfall location is given by:

$$210 \quad L(t) = \int_A \omega(t, x) d(x) dx \quad (5)$$

211 where $\omega(t, x) = \frac{R(t,x)}{\int_A R(t,x) dx}$, $d(x)$ is the linear distance from point x to the outlet. –The rainfall-weighted flow distance is:

$$212 \quad \text{RWD}(t) = \int_A \omega(t, x) d_f(x) dx \quad (6)$$

213 where distance function $d_f(x)$ is the flow distance between point x and the outlet. It is calculated as the sum of the
214 overland flow distance from x to the nearest channel and the distance along the channel to the basin outlet. The flow distance
215 $d_f(x)$ is normalized by the maximum flow distance, ranging from 0 to 1. RWD with values close to 0 indicates that rainfall
216 is distributed near the basin outlet; with values close to 1 indicates rainfall concentrated at the far periphery of the basin.

217 For a uniformly distributed rainfall, the mean RWD is:

$$218 \quad \overline{\text{RWD}} = \int_A d_f(x) dx \quad (7)$$

219 The dispersion of RWD:

$$220 \quad S(t) = \frac{1}{\bar{s}} \int_A \omega(t, x) [d_f(x) - \bar{d}]^2 dx \quad (8)$$

221 where $\bar{s} = \int_A [d_f(x) - \bar{d}]^2 dx$, S is a spatial indicator with values < 1 indicates that rainfall is a unimodal distribution, that
222 is, spatially one peak over the watershed; S with values > 1 indicates that rainfall is a multimodal distribution.
223 The Eqs.1-3 are typical rainfall characteristics used in conventional rainfall-flood analysis since they reflect the general
224 information of rainfall. Since the basin-averaged index will ignore the potential spatial heterogeneity over the watershed,
225 Eqs. 4-8 describe the spatial distribution of rainfall within the area.

226 **2.4.2 Spatiotemporal characteristics of hydrologic response**

227 Flood peak (Q_{peak} , mm^3/s), total runoff (Q_{sum} , mm), and lag time (T_{lag} , min) are defined as:

$$228 \quad Q_{peak} = \max\{Q(t); t \in T_d\} \quad (9)$$

$$229 \quad Q_{sum} = \sum_0^{T_d} Q(t) \quad (10)$$

$$230 \quad T_{lag} = T_{Fpeak} - T_{Rpeak} \quad (11)$$

231 Respectively, where $Q(t)$ is the flow discharge at time t ; T_d is the duration of hydrological response, which is from the

232 start of rainfall event to the time when $f(t) < 0.05 * Q_{peak}$.

233 3. Results and Discussion

234 3.1 Model validation

235 We validated the Dead Run GSSHA model through analyses of the 21 largest warm season (April-September) flood events
236 with peak discharges ranging from 70.3 to 253 m³/s in the 2008-2012 period. The simulated discharge was compared to
237 USGS streamflow observations for all six gaging stations. We assessed peak discharge, peak time and Nash-Sutcliffe
238 Efficiency (NSE) (Nash and Sutcliffe, 1970) to examine the performance of the model. ~~The GSSHA modeled and USGS
239 gage measured hydrographs for three storm events are compared in Fig. A2-A4 in Appendix A.~~

241 Peak discharge difference is calculated as the difference between the modeled peak and measured peak as a percentage of
242 the measured peak (Fig. 2a). ~~The peak discharge is underestimated at DR2, DR4, DR5 and Franklinton. The median peak
243 discharge difference at the downstream Franklinton gage was -14%. For the subwatersheds, the modeled peak at DR2
244 matches observation best with a median difference of -7.8%. This represents relatively good performance in reproducing
245 peak discharges for such a large collection of flood events with various peak discharges ranging from 70 m³/s to 253 m³/s.
246 The peaks at DR1 are overestimated substantially by 57% on average. Median peak discharge differences across all 21
247 events range from -35% to 57% (Fig. 2a). The largest difference is in sub-basin DR-1. ~~The reason of less fit between
248 observations and model. The issue at DR-1 was shown before in is likely that it has a large area of land which was not
249 represented fully on county storm sewer maps (Smith et al., 2015) who speculate that the watershed contains a large land
250 area which is not represented fully on county storm sewer maps. The median peak discharge difference at the watershed
251 outlet was -14%.~~~~

252 -The peak time difference is calculated as the time difference between the simulated peak time and measured peak time
253 (Fig. 2b). The median difference ranges from -15 min to +10 minutes, which is within the temporal resolution of the data
254 (15 minutes for rainfall; 5 minutes for streamflow). ~~It should be noted that there are several large peak time differences
255 occurred within the 21 storm events. These are due to the storms that produce multiple discharge peaks. The measured
256 discharge may have the first peak as the largest while the modeled discharge has the next peak as the largest which is
257 hundreds of minutes later. Nonetheless, the figure shows that the timing of the peak flow is well captured by the model.~~

258 The median Nash-Sutcliffe Efficiency (NSE) for the 21 events at Franklinton is 0.77 (Fig. 2c). The best NSE at
259 Franklinton is 0.97 indicating that the match between model and measured data was nearly exact. For the subwatersheds
260 sub-basins, the best median NSE is at DR-4 with a value of 0.74, while the least median NSE is at DR-1 with a value of

0.21. The reason of less fit between observations and model at DR-1 is likely that it has a large area of land which was not represented fully on county storm sewer maps (Smith *et al.*, 2015). The results show that the main tendency of flood response is captured by the model.

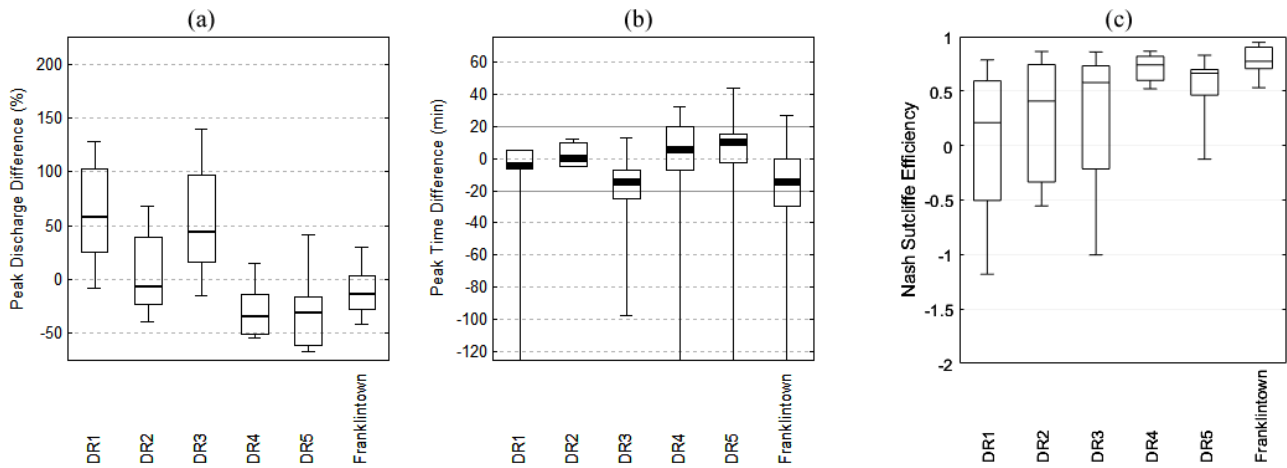


Figure 2. Comparison of (a) flood peak discharges, (b) response times and (c) NSE for 21 historical rainfall events.

The hydrograph of the 14 August 2011 storm event is shown as a representative of flood simulation. The peak discharge difference is -12% at Franklinton with a NSE of 0.93. Modeled hydrographs matches the measured data well at the outlet of watershed. For the subwatersheds, the peak discharge difference ranges from -38% at DR4 to 12% at DR-1. The shape and timing of the modeled response is similar to the measured hydrograph. But the peak discharge is underestimated by more than 30% at DR-4.

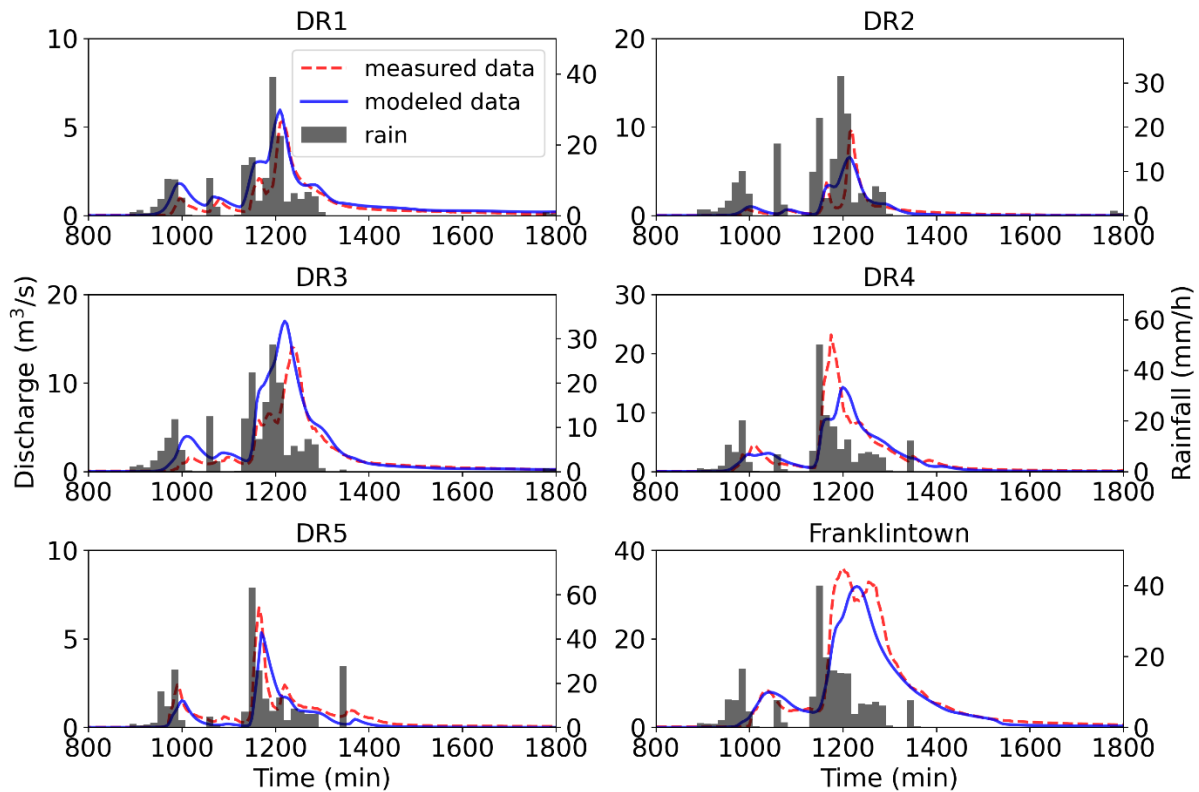


Figure 3. Hydrographs and rainfall for the the 14 August 2011 storm event. Time refers to minutes from the start of the model simulation.

It should be noted that the error in simulated response may be attributable to measurement errors tied to stage-discharge curves and to conversions of radar reflectivity to rainfall rate, as well as to the features that were simplified within the model, such as initial soil moisture and some aspects of the storm drain network (Smith *et al.*, 2015). For example, it has been documented that the average error of discharge between USGS direct measurements and stage-discharge curves for Franklinton is 17.4% between 2008 and 2010 (Lindner and Miller, 2012); this error likely grows for high flow conditions. Furthermore, for the rainfall data set used in this study, the median difference of the storm total rainfall between a rain gage and the bias-corrected radar rainfall data for all the pixel of gages over the 21 storms is 22.6% (Smith *et al.*, 2015). It may also increase the error in the measurements and modeling results. (Potter, 1981 #688) (Potter, 1985 #689) (Lindner, 2012 #690) (Smith, 2015 #126)

Overall, the validation shows that the hydrological-physically based, minimally-calibrated model can capture the main shape and timing of the measured response in Dead Run. We therefore conclude that the model is suitable for the subsequent flood frequency analysis. It should be noted that the errors in simulated response may be attributable to measurement errors tied to stage-discharge curves and to conversions of radar reflectivity to rainfall rate, as well as to the features that were

~~simplified within the model, such as initial soil moisture and some aspects of the storm drain network (Smith *et al.*, 2015).~~

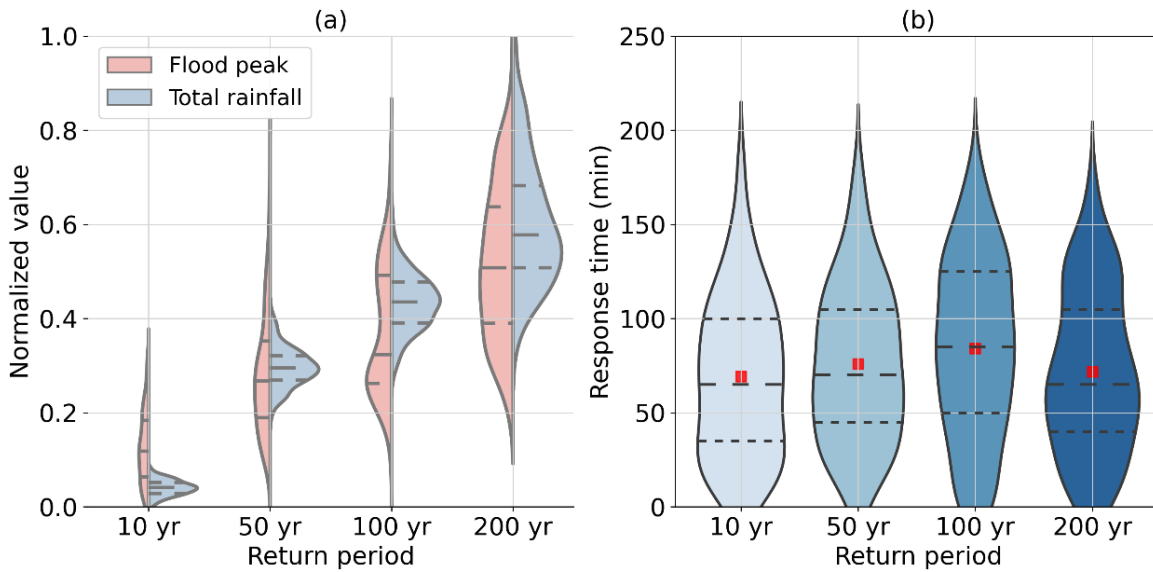
3.2 Flood frequency distribution

Under the SST framework, 3-h rainfall scenarios for 10-yr, 50-yr, 100-yr and 200-yr return periods were generated (Fig. ~~A5-A2~~ in Appendix A). ~~For each rainfall return period, 300 realizations of rainfall events are used as input to drive the hydrological model. Henceforce, for each rainfall return period, 300 flood responses can be simulated~~ ~~We then simulated hydrographs using the GSSHA model and rainfall scenarios ff~~or Franklinton and the five DR subwatershedss.

3.2.1 Flow discharge estimates

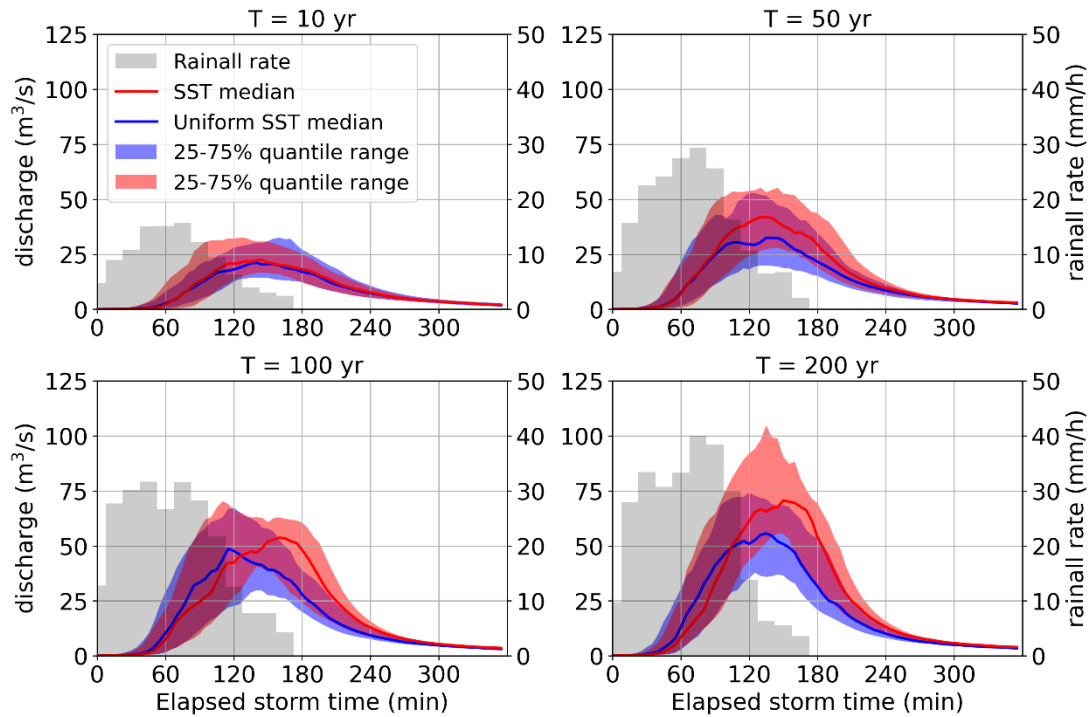
The distribution of maximum discharge at the Franklinton gage for rainfall return periods ranging from 10 to 200 years is illustrated in Fig. ~~3a4a~~. To compare the distributions of rainfall and flood peaks, the values are normalized to range from 0 to 1. ~~The normalization is the ratio of values minus the minimum to the maximum minus minimum.~~ The most striking feature is that the distributions of total rainfall and flood peaks are highly variable across the four return periods. The kernel density distribution of rainfall shows a peak at the position of 50th quantile for four return periods. The distribution of flood peak is more complex. For the 100-yr rainfall return period, the kernel density distribution of flood peaks shows a multimodal trend with two small peaks around the 25th and 75th quantiles, which contrasts with the unimodal distribution of rainfall. ~~The following results will show that flood peak is highly related to spatial rainfall features, implying that the multimodal distribution of flood peaks is associated with the spatial distribution of rainfall. For the 200-yr rainfall return period, the interquartile range (IQR) is larger than other return periods. The relative standard deviation, known as the coefficient of variation (CV), is used to present the dispersion of peak distribution. CV is defined as the ratio of the standard deviation to the mean. Unlike the IQR results, CV decreases with increasing return period. According to (Zhou *et al.*, 2019), the variability of basin average total rainfall increases with return period.~~ The pronounced difference in the distributions of total rainfall and flood peaks highlights a complex relationship between rainfall properties and flood response in this relatively small urbanized watershed.

The flood response time is calculated as the difference between the time of maximum rainfall rate and maximum discharge (Fig. ~~3b4b~~). Median values of response time are similar under all return periods, ranging from 70 to 83 minutes, which, given the temporal resolution of rainfall is 15 minutes, can be similar for all four return periods. It can be concluded that although the flood peak magnitude increases with rainfall return period, the response time is consistent for various rainfall scenarios. This implies in this small highly urbanized watershed the response time is more linked to the drainage system rather than to rainfall characteristics.



316
 317 Figure 34. Violin plots of (a) normalized flood peak and normalized total rainfall; and (b) response time based on
 318 the 3-h design storms from 10-y to 200-y rainfall return periods. (The red dot indicates mean value. Dashed line in
 319 the middle indicates the median value. Upper and lower dashed lines indicate the 75th and 25th quantiles,
 320 respectively.) The rainfall return periods are calculated with respect to average rainfall rate over the entire DR
 321 watershed.

322
 323 Figure 4-5 demonstrates the simulated hydrographs for the four return periods. The upper and lower spread (75th and 25th
 324 quantiles) of the hydrograph indicates the range of variability of simulated hydrographs. For the 10-yr return period, the
 325 hydrograph is relatively smooth with smaller spread. With increasing return period, the hydrograph is peakier with shorter
 326 duration of high magnitude discharge. The hydrograph for the 50-yr return period shows a transitional shape between small
 327 (10-yr) and large (100-yr and 200-yr) rainfall return periods. For the 100-yr return period, the upper spread shows a
 328 tendency toward dual peaks, which cannot be revealed from conventional design flood practices. Since in the conventional
 329 rainfall flood frequency approach, the design storm is temporally idealized as a unimodal peak process. By using these
 330 design storm, the flood response is generally simulated as a unimodal peak process. The above results imply the uncertainty
 331 and insufficiency of flood frequency analysis in the conventional method. For the 200-yr return period, the hydrograph is
 332 peakiest with a large upper spread.



333 **Figure 45.** Time series of simulated hydrographs for Franklinton based on the 3-h design storms from 10-yr to
 334 **200-yr return periods with spatially uniform (blue) and spatially distributed (red) rainfall. The grey bar indicates**
 335 **the median value of basin-averaged rainfall rate.**
 336

338 3.2.2 Spatial distribution of flood magnitude

339 The distribution of flood peaks over the five subwatersheds exhibits contrasting variation with rainfall return periods
 340 ranging from 10 to 200 years (Fig. 56). Generally, basin scale plays an important role in determining the distribution of
 341 flood magnitudes. Under the 10-yr rainfall return period, DR1 and DR2, with similar basin scales of 1.32 and 2.01.92
 342 km². respectively. have higher flood peaks and interquartile ranges than other subwatersheds. DR5 (2.4-05 km²) has
 343 comparable flood magnitude with DR4 (6.3 km²) and Franklinton (14.3 km²), while has a a-larger interquartile range than
 344 the latter two. DR3 with a basin scale of 4.95 km², has comparable flood magnitudes with DR1 and DR2. Under the 200-
 345 yr rainfall return period, DR2 and DR3 has a slightly larger flood magnitude than DR1. DR5 has the largest interquartile
 346 range than others, though its flood peaks are smaller than other small watersheds.

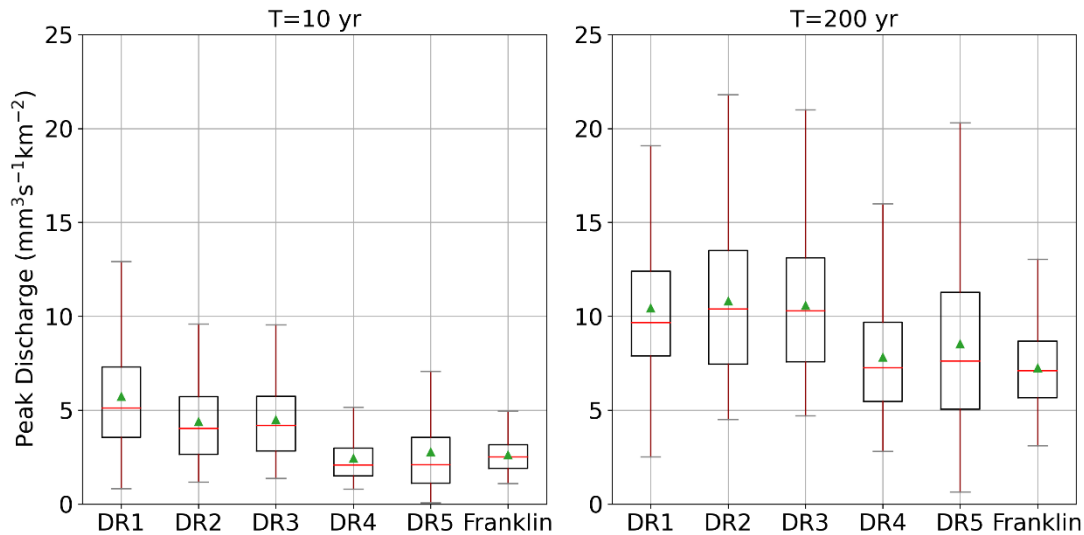
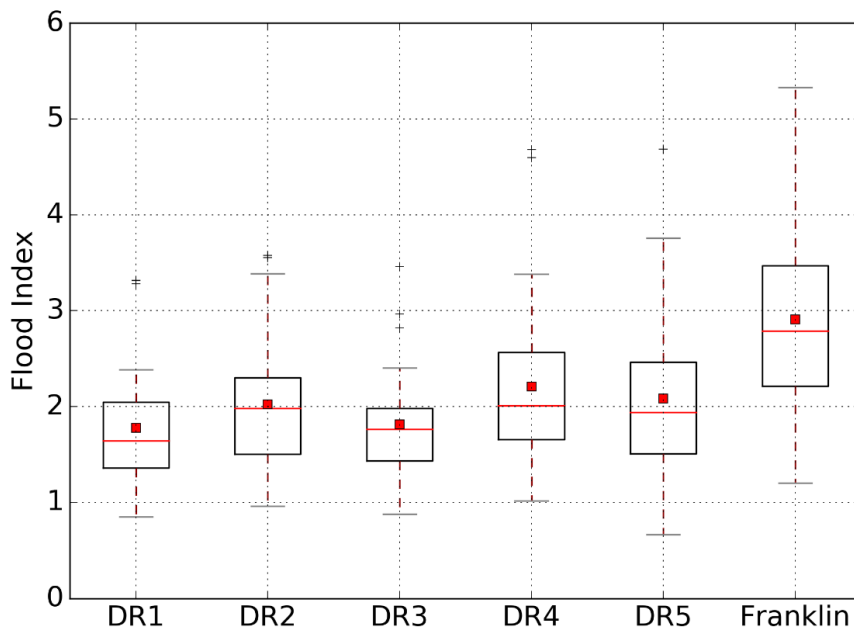


Figure 56. Boxplots of normalized flood peaks for Franklinton and five subwatersheds.

Results show that sub-basin flood distributions vary significantly with rainfall return periods. DR1 with 33% larger impervious area and more than double of detention controlled area than DR2 (Table 1), ~~h~~ has 26% larger median flood peaks under small-small rainfall return period. ~~F~~ For large return periods, DR2 has a slightly larger median peak and a ~~DR2 has~~ larger peak and interquartile range than DR1. The contrasting peaks in DR1 and DR2, implying imply that flood peaks are less impacted by impervious area for extreme storms whil for small rainfall events, detention infrastruture may play a less role in the detention of flood peaks. ~~s~~ DR5, with the smallest detention controlled area by detention infrastructure, has the smallest flood peaks under small rainfall return period. Under large return period, however, it has the largest changes in peak discharges with comparable flood peaks with subwatersheds larger than 6 km². DR3 and DR4, with basin scale of 4.95 and 6.29 km², have contrasting flood magnitude under small and large return periods. DR3 with larger impervious area and detention controlled area has larger flood peaks than DR4. The difference is more significant for small rainfall events with the median value of flood peak for DR3 more than double that of DR4. From these results, it ~~can be concluded~~ implies that impervious area and detention controlled area play a significant role in determining the peak discharges, but the impact reduces with increasing rainfall return period. ~~The less detention controlled sub-basin has larger flood variability under large return period.~~ The detention infrastructure impacts flood peak and its variability. It should be noted that difficulties remain in attributing specific changes in urban flood peak distributions to specific urbanization characteristics (Zhou *et al.*, 2017). The role of specific urban features in flood responses is beyond the scope of this paper.

We further examine the spatial distribution of flood magnitude over the Dead Run watershed under the 100-yr return period

368 of flood at Franklinton (Fig. 67). The dimensionless flood index is used to compare flood peak magnitudes over the
 369 watershed (Lu *et al.*, 2017). The flood index is computed as the maximum flow discharge divided by the computed 10-yr
 370 flood (Q_{10-y}) at the same location, which is set as the median value of 10-yr peak discharge at the watershed outlet for each
 371 100-yr design storm simulation. At Franklinton, the flood index and its interquartile range are largest across the
 372 watersheds, with the median value greater than 2.5. The flood index in the five sub-watersheds is relatively lower, within
 373 a median value between 1.5 and 2. DR2, as a sub-watershed of DR3, has a larger median value than DR1 and DR3. The
 374 flood indices at DR1 and DR3 have similar median values and interquartile ranges. Values in DR4 are higher than its sub-
 375 watershed, DR5, with a median value of 2. The variability of flood magnitudes, indicated by the CV, is stable among the
 376 watersheds, ranging from 0.30 to 0.39. The spatial distribution of flood magnitude points to the significant heterogeneity
 377 of flood distributions over the 14.3-km² watershed. For storm events that produce the same peak discharge return period at
 378 the watershed outlet, the subsequent upstream flood response can vary substantially in the Dead Run watershed.



379
 380 Figure 6.7. Boxplot of flood index across the DR subwatersheds for the 100-yr design storms.

381
 382 **3.3 Rainfall-Flood Relationships**

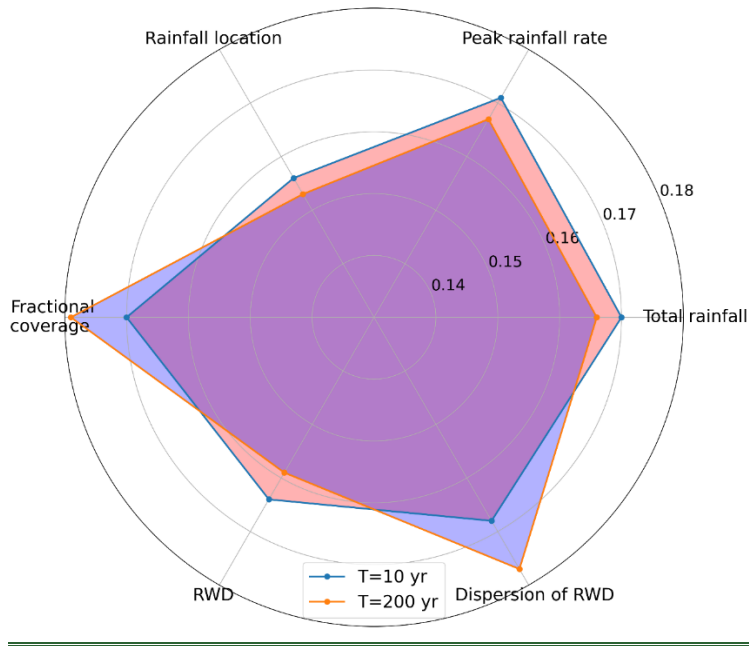
383 **3.3.1 Rainfall structure and flood response**

384 We investigate the relationship between the spatial and temporal characteristics of rainfall and flood response for small and
 385 large rainfall return periods based on Spearman's rank correlation (Fig. A36 in Appendix A). The peak rainfall rate (M_{max}),

386 total rainfall (R_{sum}), fractional coverage (Z), rainfall location (L), rainfall-weighted flow distance (RWD) and the dispersion
387 of RWD (S) are used to characterize rainfall spacetime structure. For the 10-yr return period, the flood peak is ~~somewhat~~
388 ~~slightly~~ correlated with total rainfall, peak rainfall rate and storm core coverage with correlation coefficient of 0.16. For
389 the 200-yr return period, in contrast, there is no significant correlation between these features with correlation coefficients
390 of -0.09, 0.07 and -0.02, respectively, implying a complex and nonlinear relationship between extreme storms and floods
391 in the watershed.

392 We used random forest regression models to examine the importance of rainfall characteristics to the flood response.
393 ~~Random forests (RF) is an ensemble learning method (Breiman, 2001) that aggregates results from multiple models to~~
394 ~~achieve better accuracy. RF is one of the most widely-used method for regression and classification. Moreover, it is~~
395 ~~relatively easy to train and tests. In this study, R~~rainfall spacetime structure characteristics are used as RF model features.
396 ~~{Breiman, 2001 #465}~~The flood peak is set as the model target. ~~The relationship between rainfall structure and flood peak~~
397 ~~is then explored under the RF-based regression method.~~ The main parameters of RF model are tuned by a grid search
398 approach (Probst *et al.*, 2019). The prediction performance is assessed using Mean Absolute Error (MAE), Root Mean
399 Square Error ($RMSE$), and explained variance regression score (E score) (Achen, 2017). Smaller values of MAE and $RMSE$
400 indicate better model performance. E score ranges from 0 to 1 and a larger value indicates a better model (The training
401 process of RF model is shown in Fig. A47 in Appendix A).

402 The difference in feature importance is compared between the 10-yr and 200-yr return periods (Fig. 87). For the 10-yr
403 return period, peak rainfall rate (M_{max}) and total rainfall (R_{sum}) are the most two important features ~~with feature importance~~
404 ~~of 0.17~~. For the 200-yr return period, however, the dispersion of RWD (S) and fractional coverage of storm core (Z) are
405 more important than ~~M_{max} peak rainfall rate~~ and ~~R_{sum} total rainfall~~. The rainfall location (L) has the smallest importance for
406 both return periods. The results demonstrate the different relationships between rainfall structure and flood response under
407 small and extreme rainfall events. For extreme storms, the maximum discharge is more closely linked to the spatial structure
408 of rainfall, which is consistent with the results in ~~{Peleg, 2017 #313}~~; ~~{Peleg *et al.*, 2017; Zhu *et al.*, 2018}~~ {Zhu, 2018
409 #584}. ~~Though it appears that the difference is moderate, but for a such small watershed, the tendency of the change of~~
410 ~~spatiotemperol rainfall feature importance is noteworthy.~~

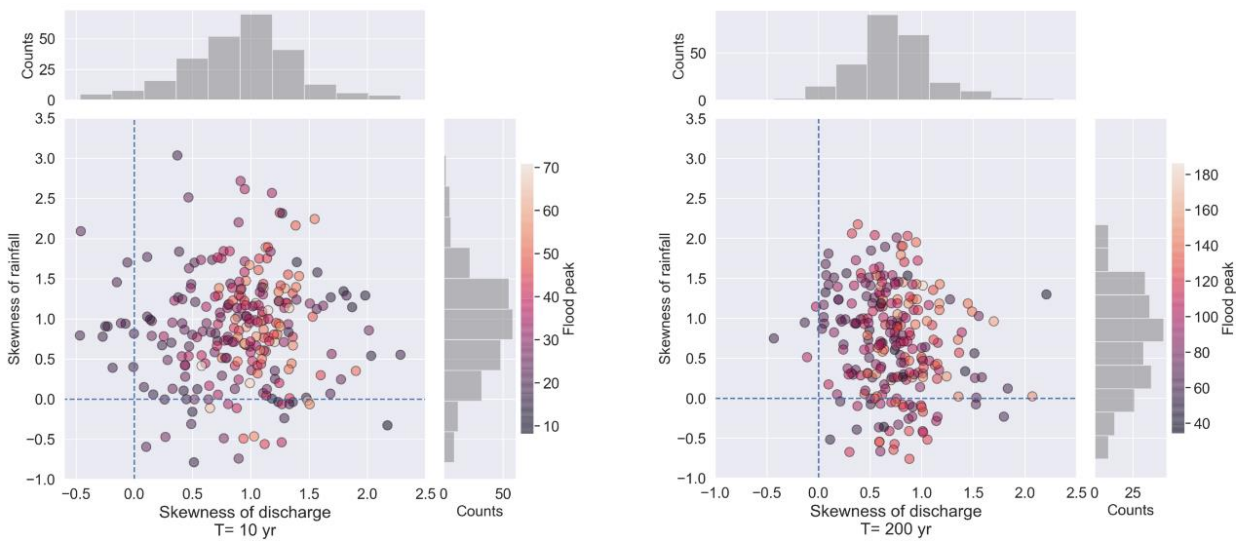


411

412 **Figure 87. Feature importance analysis of RF model for space-time rainfall structure and 10-yr (red) and 200-yr**
 413 **(blue) flood peaks.**

414

415 The temporal shapes of hydrographs and hietographs are compared by using the coefficient of skewness (Fig. 8). The
 416 skewness is used to assess the shape of rainfall process and discharge process. A negative value of skew indicates a left tail
 417 of the distribution, and positive indicates a right tail. For the 10 yr return period, the rainfall skewness ranges from -0.1 to
 418 3.5, demonstrating the mixed shapes of temporal distribution. Similar features are found for discharge shapes. For the 200-
 419 yr return periods, the skewness of discharge is mostly positive while the skewness of rainfall events still varies from -1 to
 420 2.5. The general conclusion of these analyses is that regardless of the temporal distribution of rainfall, the flood response
 421 is relatively rapid, highlighting the role of the urban drainage system for the hydrographic response. The relationship
 422 between the variability of discharge and rainfall is not significant for the four return periods, which implies that in a highly-
 423 urbanized watershed, the drainage system smooths rainfall variability somewhat.



424

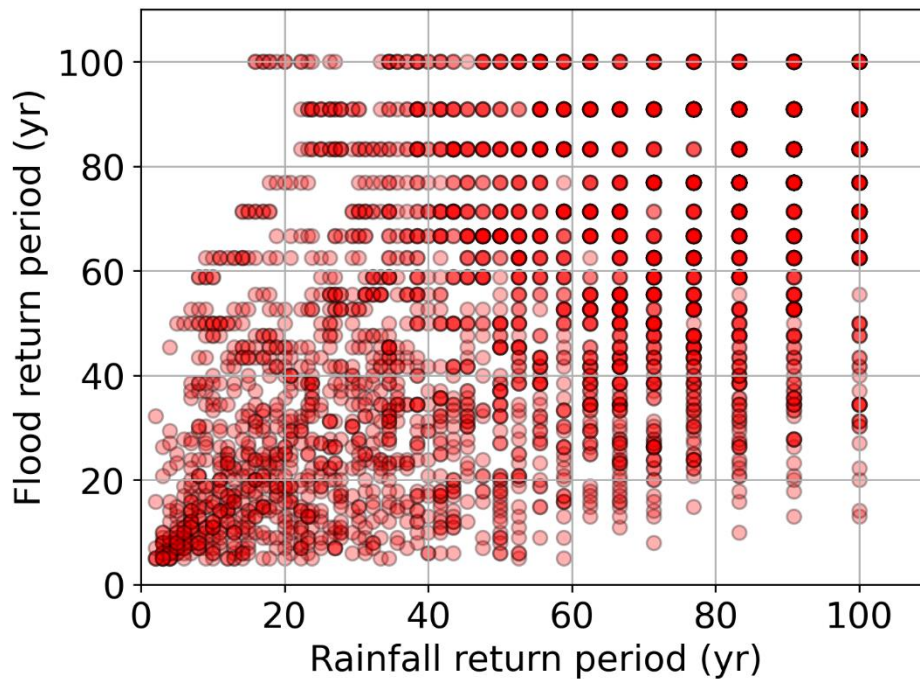
425 **Figure 8. Scatter plots of skewness of rainfall and peak discharge — left: 10-yr return period; right: 200-yr return**

426 period.

427

428 3.3.2 Rainfall return period vs. flood return period

429 In conventional design storm/flood practices, the return period of rainfall and peak discharge is often assume to be
430 equivalent (Rahman *et al.*, 2002). Under the SST framework, we can examine this assumption (Wright *et al.*, 2014a). At
431 the 14.3-km² basin scale, Ffor each SST realization containing 100 rainfall scenarios with return period from 5 years up to
432 100 years, the peak discharge can be simulated and ordered. Flood frequency for return periods from 5 years up to 100
433 years are then estimated from the ordered peaks. We run 30 SST realizations in total. The Spearman's rank correlation of
434 the two return periods is 0.5 (Fig. 99). The results quantitatively confirm that the assumption of a 1:1 return period
435 equivalency between design storm and design flood cannot hold, even in a small highly-urbanized watershed where
436 drainage network and rainfall structure play an important role in flood response. Similar results can be found between
437 subbasins flood and DR-scale rainfall return periods (results not shown for the sake of brevity).



438

439 Figure 9. Scatterplot comparison return periods for rainfall and peak discharge for individual SST-based
440 simulations.

441

442 3.3.3 Impact of rainfall spatial heterogeneity on flood responses

443 We also compared the simulated flood response resulting when rainfall is uniform over the watershed, rather than spatially

distributed as in previous analyses (Fig. 4 and Table 2). Generally, the flood peaks generated from uniform rainfall have lower peaks than for non-uniform rainfall. The difference increases with return period. Under the 10-yr return period, the shapes of the two hydrographs have similar upper and lower bounds (75% and 25% quantiles). The median flood peak using non-uniform scenarios is 22% higher than the uniform scenarios. Under the 200-yr return period, the hydrograph resulting from non-uniform rainfall is much peakier than the uniform SST scenarios with higher upper and lower bounds. The lower bound of hydrograph by non-uniform SST scenarios is close to the median hydrograph of uniform SST scenarios. The impact of rainfall spatial heterogeneity among the five subwatersheds is different. DR1, with a basin scale of 1.32 km² and located in the north-west boundary of the watershed, was the least-impacted by rainfall spatial distribution for all return periods. In DR2, on the other hand, which is similar in drainage area to DR1, the flood peak increased by 46% for the 200-yr return period. For DR3 and DR4, the spatial heterogeneity of rainfall contributes more to the flood peaks in DR4 than in DR3. The most striking difference in flood peaks is in DR5 for the 50-yr return period. The difference in flood magnitude is 75%. As mentioned above, DR5 is the sub-basin with the least detention controlled area. This finding is likely tied to the complex relationship between space-time rainfall structure and the drainage network. We can thus conclude that the spatial heterogeneity of rainfall can increase flood peaks dramatically under both small and large return periods. The impact increases with return period. This result shows that the assumption of spatially uniform rainfall will underestimate flood frequency.

Table 2. The median flood peak reductions using spatially uniform and spatially distributed rainfall.

	<u>T=10 yr</u>	<u>T=50 yr</u>	<u>T=100 yr</u>	<u>T=200 yr</u>
<u>DR1</u>	<u>14%</u>	<u>20%</u>	<u>13%</u>	<u>26%</u>
<u>DR2</u>	<u>19%</u>	<u>40%</u>	<u>28%</u>	<u>42%</u>
<u>DR3</u>	<u>24%</u>	<u>33%</u>	<u>27%</u>	<u>31%</u>
<u>DR4</u>	<u>32%</u>	<u>51%</u>	<u>38%</u>	<u>35%</u>
<u>DR5</u>	<u>15%</u>	<u>75%</u>	<u>37%</u>	<u>30%</u>
<u>Franklin</u>	<u>22%</u>	<u>36%</u>	<u>31%</u>	<u>42%</u>

4. Summary and conclusions

This paper addresses the problem of the impacts of short-duration rainfall variability on hydrologic response in small urbanized watershed. By coupling a high-resolution radar rainfall dataset and stochastic storm transposition (SST) with the GSSHA distributed physics-based model (see also (Wright *et al.*, 2014a; Zhu *et al.*, 2018)), the relationships between rainfall spatiotemporal structure and urban flood response is examined. The main findings are as follows:

467 1. The flood frequency distributions for subwatersheds within the highly-urbanized 14.3-km² Dead Run watershed
468 demonstrates ~~the complexities~~ of flood response for both short and long rainfall return periods. ~~Especially for~~ 3-h
469 extreme storms, the ~~distribution of flood peaks shows large variability. The large~~ variability of flood magnitude shows a
470 pronounced role of rainfall space-time structure in flood production. This calls into question the commonly-made design
471 storm assumption of spatially uniform rainfall. The response time is less affected by rainfall structure and appears to be
472 more closely associated with the basin scale and drainage network features.

473 2. The spatial heterogeneity of flood frequency over the 14.3-km² watershed is striking for the 100-yr return period. The
474 intercomparison between subwatersheds show that the impact of impervious area decreases with increasing return periods.
475 ~~The subbasin with the least detention infrastructure shows the largest flood variability for long return periods.~~ For the 100-
476 yr return period, ~~the flood index of five subwatersheds are different from that of their downstream outlet. It shows that~~
477 storm events that produce the same peak discharge return period at the basin outlet can be the result of very different
478 upstream flood responses even in a small-scale watershed.

479 3. The relationship between the spacetime structure of rainfall and flood response is complex. ~~The random forest based~~
480 ~~feature importance analysis shows very different relationships between rainfall structure and flood response for frequent~~
481 ~~vs. extreme rainfall events.~~ For smaller and more frequent rainfall events, flood peaks are more closely linked to the
482 temporal features of rainfall (total rainfall and peak rainfall rate). For extreme storms, the maximum discharge is closely
483 linked to the spatial structure of rainfall (storm core coverage). This finding is broadly consistent with Peleg *et al.* (2017)
484 and Zhu *et al.* (2018), despite the very different drainage scales considered in those studies. There is no significant
485 correlation between rainfall peak, total rainfall and flood peaks, implying an important role of surface properties in
486 urbanized watersheds. Similar to Wright *et al.* (2014a), this comparison calls into question the conventional design storm
487 assumption of a 1:1 equivalency between rainfall and flood peak return periods.

488 4. The spatial heterogeneity of rainfall is a key driver of flood response across scales. Relative to spatially uniform rainfall,
489 spatially distributed rainfall can increase flood peaks by 50% on average at the watershed outlet and its subwatersheds for
490 both small and large return periods. This finding is broadly consistent with prior results at much larger scales in an
491 agricultural setting (~~Zhu *et al.* (2018)~~) and suggests both spatial and temporal rainfall distributions need to be considered
492 in flood frequency analyses, even in relatively small urban watersheds. This study also implies that the drainage network
493 substantially alters the impact of rainfall characteristics on the runoff.

494 Coupling the GSSHA model and SST-based rainfall frequency analysis, this study provides an effective approach for
495 regional flood frequency analysis for urban watersheds. Some idealized assumptions used in the conventional methods are
496 questioned. ~~The approach~~ can be used to explore the dominant control on the upper tail of urban flood peaks, without

497 many of the limiting assumptions associated with design storm methods. The study area could be extended in future work
498 with larger basin scales and by manipulating the spatial heterogeneity of basin characteristics within GSSHA or other
499 similar modeling systems.

500 **Acknowledgments**

501 This study was supported by the National Science Foundation of China (Grant 51909191).

502 **Data availability**

503 Radar data are archived at Princeton University and can be downloaded from the url
504 <http://arks.princeton.edu/ark:/88435/dsp01q524jr55d>.

505

506 **Author contributions**

507 Main contributions from each co-authors are as follows. Zhengzheng Zhou contributed to computation and organization of
508 the paper. James A. Smith contributed to the supervision and writing. Mary Lynn Beack is responsible for generating the
509 radar rainfall data. Brianne K. Smith contributed to the construction of the initial hydrological model. Daniel B. Wright
510 contributed to the writing of the paper. Shuguang Liu contributed to the supervision and writing.

511

512

Reference

513

514 Achen, C. H. (2017), What Does “Explained Variance“ Explain?: Reply, *Political Analysis*, 2, 173-
515 184. doi:10.1093/pan/2.1.173

516 Adams, R., A. W. Western, and A. W. Seed (2012), An analysis of the impact of spatial variability in
517 rainfall on runoff and sediment predictions from a distributed model, *Hydrological Processes*, 26(21),
518 3263-3280. doi:10.1002/hyp.8435

519 Beighley, R. E., and G. E. Moglen (2002), Trend Assessment in Rainfall-Runoff Behavior in
520 Urbanizing Watersheds, *Journal of Hydrologic Engineering*, 7(1), 27-34. doi:10.1061/(ASCE)1084-
521 0699(2002)7:1(27)

522 Berne, A., G. Delrieu, J.-D. Creutin, and C. Obled (2004), Temporal and spatial resolution of rainfall
523 measurements required for urban hydrology, *Journal of Hydrology*, 299(3), 166-179.
524 doi:10.1016/j.jhydrol.2004.08.002

525 Breiman, L. (2001), Random Forests, *Machine Learning*, 45(1), 5-32. 10.1023/a:1010933404324

526 Bruni, G., R. Reinoso, d. G. Van, N. C., F. H. L. R. Clemens, and J. A. E. Ten Veldhuis (2015), On the
527 sensitivity of urban hydrodynamic modelling to rainfall spatial and temporal resolution, *Hydrology
528 and Earth System Sciences*, 19(2), 691-709. doi:10.5194/hess-19-691-2015, 2015

529 Cristiano, E., M. C. ten Veldhuis, and N. van de Giesen (2017), Spatial and temporal variability of
530 rainfall and their effects on hydrological response in urban areas – a review, *Hydrology and Earth
531 System Siences*, 21(7), 3859-3878. doi:10.5194/hess-21-3859-2017

532 Cristiano, E., M. C. ten Veldhuis, S. Gaitan, S. Ochoa Rodriguez, and N. van de Giesen (2018), Critical
533 scales to explain urban hydrological response: an application in Cranbrook, London, *Hydrol. Earth*
534 *Syst. Sci.*, 22(4), 2425-2447. doi:10.5194/hess-22-2425-2018

535 Cristiano, E., M.-c. ten Veldhuis, D. B. Wright, J. A. Smith, and N. van de Giesen (2019), The Influence
536 of Rainfall and Catchment Critical Scales on Urban Hydrological Response Sensitivity, *Water*
537 *Resources Research*, 55(4), 3375-3390. doi:10.1029/2018WR024143

538 Downer, C. W., and F. L. Ogden (2004), GSSHA: Model to simulate diverse stream flow producing
539 processes, *Journal of Hydrologic Engineering*, 9(3), 161-174. doi:10.1061/(ASCE)1084-
540 0699(2004)9:3(161)

541 Downer, C. W., and F. L. Ogden (2006), Gridded Surface Subsurface Hydrologic Analysis (GSSHA)
542 User's Manual; Version 1.43 for Watershed Modeling System 6.1.

543 Emmanuel, I., H. Andrieu, E. Leblois, and B. Flahaut (2012), Temporal and spatial variability of
544 rainfall at the urban hydrological scale, *Journal of Hydrology*, 430-431, 162-172.
545 doi:10.1016/j.jhydrol.2012.02.013

546 Emmanuel, I., H. Andrieu, E. Leblois, N. Janey, and O. Payrastre (2015), Influence of rainfall spatial
547 variability on rainfall-runoff modelling: Benefit of a simulation approach?, *Journal of Hydrology*, 531,
548 337-348. doi:10.1016/j.jhydrol.2015.04.058

549 Faurès, J.-M., D. C. Goodrich, D. A. Woolhiser, and S. Sorooshian (1995), Impact of small-scale spatial
550 rainfall variability on runoff modeling, *Journal of Hydrology*, 173(1), 309-326. doi:10.1016/0022-
551 1694(95)02704-S

552 Fulton, R. A., J. P. Breidenbach, D.-J. Seo, D. A. Miller, and T. O'Bannon (1998), The WSR-88D
553 rainfall algorithm, *Weather and Forecasting*, 13(2), 377-395. doi:10.1175/1520-
554 0434(1998)013<0377:TWRA>2.0.CO;2

555 Galster, J. C., F. J. Pazzaglia, B. R. Hargreaves, D. P. Morris, S. C. Peters, and R. N. Weisman (2006),
556 Effects of urbanization on watershed hydrology: The scaling of discharge with drainage area, *Geology*,
557 34(9), 713-716. doi:10.1130/g22633.1

558 Gebremichael, M., and W. F. Krajewski (2004), Assessment of the statistical characterization of small-
559 scale rainfall variability from radar: Analysis of TRMM ground validation datasets, *Journal of Applied*
560 *Meteorology*, 43(8), 1180-1199. doi:10.1175/1520-0450(2004)043<1180:AOTSCO>2.0.CO;2

561 Gesch, D. B., M. J. Oimoen, S. K. Greenlee, C. A. Nelson, M. J. Steuck, and D. J. Tyler (2002), The
562 national elevation data set, *Photogrammetric Engineering and Remote Sensing*, 68(1), 5-11.

563 Gourley, J. J., et al. (2017), The FLASH Project: Improving the Tools for Flash Flood Monitoring and
564 Prediction across the United States, *Bulletin of the American Meteorological Society*, 98(2), 361-372.
565 doi:10.1175/bams-d-15-00247.1

566 Krajewski, W., and J. Smith (2002), Radar hydrology: rainfall estimation, *Advances in water resources*,
567 25(8-12), 1387-1394. doi:10.1016/S0309-1708(02)00062-3

568 Krajewski, W. F., A. Kruger, J. A. Smith, R. Lawrence, C. Gunyon, R. Goska, B.-C. Seo, P.
569 Domaszczynski, M. L. Baeck, and M. K. Ramamurthy (2011), Towards better utilization of NEXRAD
570 data in hydrology: an overview of Hydro-NEXRAD, *Journal of hydroinformatics*, 13(2), 255-266.
571 doi:10.2166/hydro.2010.056

572 Lin, N., J. A. Smith, G. Villarini, T. P. Marchok, and M. L. Baeck (2010), Modeling extreme rainfall,
573 winds, and surge from Hurricane Isabel (2003), *Weather and forecasting*, 25(5), 1342-1361.
574 doi:10.1175/2010WAF2222349.1

575 Lindner, G. A., and A. J. Miller (2012), Numerical modeling of stage-discharge relationships in urban

576 streams, *Journal of Hydrologic Engineering*, 17(4), 590-596.

577 Lu, P., J. A. Smith, and N. Lin (2017), Spatial Characterization of Flood Magnitudes over the Drainage
578 Network of the Delaware River Basin, *Journal of Hydrometeorology*, 18(4), 957-976.
579 doi:10.1175/jhm-d-16-0071.1

580 Maryland, S. o. (1982), Department of the Environment : Water management, stormwater management.

581 Meierdiercks, K. L., J. A. Smith, M. L. Baeck, and A. J. Miller (2010), Analyses of urban drainage
582 network structure and its impact on hydrologic response, *JAWRA Journal of the American Water
583 Resources Association*, 46(5), 932-943.

584 Moreau, E., J. Testud, and E. Le Bouar (2009), Rainfall spatial variability observed by X-band weather
585 radar and its implication for the accuracy of rainfall estimates, *Advances in Water Resources*, 32(7),
586 1011-1019. doi:10.1016/j.advwatres.2008.11.007

587 Morin, E., D. C. Goodrich, R. A. Maddox, X. Gao, H. V. Gupta, and S. Sorooshian (2006), Spatial
588 patterns in thunderstorm rainfall events and their coupling with watershed hydrological response,
589 *Advances in Water Resources*, 29(6), 843-860.

590 Nash, J. E., and J. V. Sutcliffe (1970), River flow forecasting through conceptual models part I — A
591 discussion of principles, *Journal of Hydrology*, 10(3), 282-290. [https://doi.org/10.1016/0022-
592 1694\(70\)90255-6](https://doi.org/10.1016/0022-1694(70)90255-6)

593 Nelson, P. A., J. A. Smith, and A. J. Miller (2006), Evolution of channel morphology and hydrologic
594 response in an urbanizing drainage basin, *Earth Surface Processes and Landforms*, 31(9), 1063-1079.
595 doi:10.1002/esp.1308

596 Nikolopoulos, E. I., M. Borga, D. Zoccatelli, and E. N. Anagnostou (2014), Catchment-scale storm
597 velocity: Quantification, scale dependence and effect on flood response, *Hydrological Sciences
598 Journal*, 59(7), 1363-1376. doi:10.1080/02626667.2014.923889

599 Ntelekos, A. A., J. A. Smith, M. L. Baeck, W. F. Krajewski, A. J. Miller, and R. Goska (2008), Extreme
600 hydrometeorological events and the urban environment: Dissecting the 7 July 2004 thunderstorm over
601 the Baltimore MD Metropolitan Region, *Water Resources Research*, 44(8), 1-19.
602 doi:10.1029/2007WR006346

603 Ochoa-Rodriguez, S., L.-P. Wang, A. Gires, R. D. Pina, R. Reinoso-Rondinel, G. Bruni, A. Ichiba, S.
604 Gaitan, E. Cristiano, and J. van Assel (2015), Impact of spatial and temporal resolution of rainfall
605 inputs on urban hydrodynamic modelling outputs: A multi-catchment investigation, *Journal of
606 Hydrology*, 531(2), 389-407. doi:10.1016/j.jhydrol.2015.05.035

607 Ogden, F. L., N. Raj Pradhan, C. W. Downer, and J. A. Zahner (2011), Relative importance of
608 impervious area, drainage density, width function, and subsurface storm drainage on flood runoff from
609 an urbanized catchment, *Water Resources Research*, 47(12). doi:10.1029/2011wr010550

610 Paschalis, A., S. Fatichi, P. Molnar, S. Rimkus, and P. Burlando (2014), On the effects of small scale
611 space–time variability of rainfall on basin flood response, *Journal of Hydrology*, 514, 313-327.
612 doi:10.1016/j.jhydrol.2014.04.014

613 Peleg, N., F. Blumensaat, P. Molnar, S. Fatichi, and P. Burlando (2017), Partitioning the impacts of
614 spatial and climatological rainfall variability in urban drainage modeling, *Hydrology and Earth System
615 Sciences*, 21(3), 1559. doi:10.5194/hess-21-1559-2017

616 Perez, G., R. Mantilla, W. F. Krajewski, and D. B. Wright (2019), Using Physically Based Synthetic
617 Peak Flows to Assess Local and Regional Flood Frequency Analysis Methods, *Water Resources
618 Research*, 55(11), 8384-8403. doi:10.1029/2019WR024827

619 Pickett, S. T. A., and M. L. Cadenasso (2006), Advancing urban ecological studies: Frameworks,

620 concepts, and results from the Baltimore Ecosystem Study, *Austral Ecology*, 31(2), 114-125.
621 doi:10.1111/j.1442-9993.2006.01586.x

622 Probst, P., M. N. Wright, and A. L. Boulesteix (2019), Hyperparameters and tuning strategies for
623 random forest, *Wiley Interdisciplinary Reviews: Data Mining and Knowledge Discovery*, 9(3), e1301.
624 doi:10.1002/widm.1301

625 Rafieeinassab, A., A. Norouzi, S. Kim, H. Habibi, B. Nazari, D.-J. Seo, H. Lee, B. Cosgrove, and Z.
626 Cui (2015), Toward high-resolution flash flood prediction in large urban areas – Analysis of sensitivity
627 to spatiotemporal resolution of rainfall input and hydrologic modeling, *Journal of Hydrology*, 531,
628 370-388. doi:10.1016/j.jhydrol.2015.08.045

629 Rahman, A., P. E. Weinmann, T. M. T. Hoang, and E. M. Laurenson (2002), Monte Carlo simulation
630 of flood frequency curves from rainfall, *Journal of Hydrology*, 256(3), 196-210. doi:10.1016/S0022-
631 1694(01)00533-9

632 Saghafian, B., P. Y. Julien, and F. L. Ogden (1995), Similarity in catchment response: 1. Stationary
633 rainstorms, *Water Resources Research*, 31(6), 1533-1541. doi:10.1029/95WR00518

634 Schellart, A. N. A., W. J. Shepherd, and A. J. Saul (2012), Influence of rainfall estimation error and
635 spatial variability on sewer flow prediction at a small urban scale, *Advances in Water Resources*, 45,
636 65-75. doi:10.1016/j.advwatres.2011.10.012

637 Seo, B.-C., W. F. Krajewski, A. Kruger, P. Domaszczynski, J. A. Smith, and M. Steiner (2011), Radar-
638 rainfall estimation algorithms of Hydro-NEXRAD, *Journal of Hydroinformatics*, 13(2), 277-291.
639 doi:10.2166/hydro.2010.003

640 Sharif, H. O., A. A. Hassan, S. Bin-Shafique, H. Xie, and J. Zeitler (2010), Hydrologic modeling of
641 an extreme flood in the Guadalupe River in Texas, *JAWRA Journal of the American Water Resources
642 Association*, 46(5), 881-891. doi:10.1111/j.1752-1688.2010.00459.x

643 Sharif, H. O., S. Chintalapudi, A. A. Hassan, H. Xie, and J. Zeitler (2013), Physically Based
644 Hydrological Modeling of the 2002 Floods in San Antonio, Texas, *Journal of Hydrologic Engineering*,
645 18(2), 228-236. doi:10.1061/(ASCE)HE.1943-5584.0000475

646 Smith, B., J. Smith, M. Baeck, and A. Miller (2015), Exploring storage and runoff generation processes
647 for urban flooding through a physically based watershed model, *Water Resources Research*, 51(3),
648 1552-1569. doi:10.1002/2014WR016085

649 Smith, B. K., J. A. Smith, M. L. Baeck, G. Villarini, and D. B. Wright (2013), Spectrum of storm event
650 hydrologic response in urban watersheds, *Water Resources Research*, 49(5), 2649-2663.
651 doi:10.1002/wrcr.20223

652 Smith, J. A., and W. F. Krajewski (1991), Estimation of the mean field bias of radar rainfall estimates,
653 *Journal of Applied Meteorology*, 30(4), 397-412.

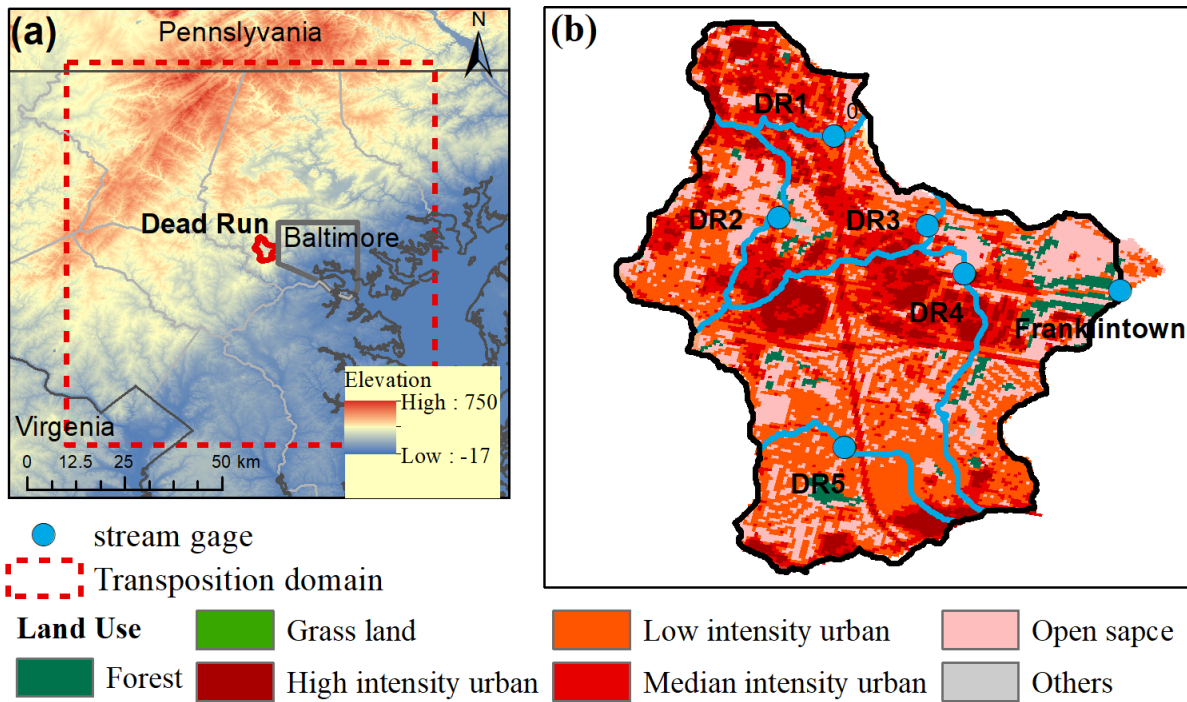
654 Smith, J. A., M. L. Baeck, K. L. Meierdiercks, A. J. Miller, and W. F. Krajewski (2007), Radar rainfall
655 estimation for flash flood forecasting in small urban watersheds, *Advances in Water Resources*, 30(10),
656 2087-2097. doi:10.1016/j.advwatres.2006.09.007

657 Smith, J. A., M. L. Baeck, J. E. Morrison, P. Sturdevant-Rees, D. F. Turner-Gillespie, and P. D. Bates
658 (2002), The regional hydrology of extreme floods in an urbanizing drainage basin, *Journal of
659 Hydrometeorology*, 3(3), 267-282. doi:10.1175/1525-7541(2002)003<0267:TRHOEF>2.0.CO;2

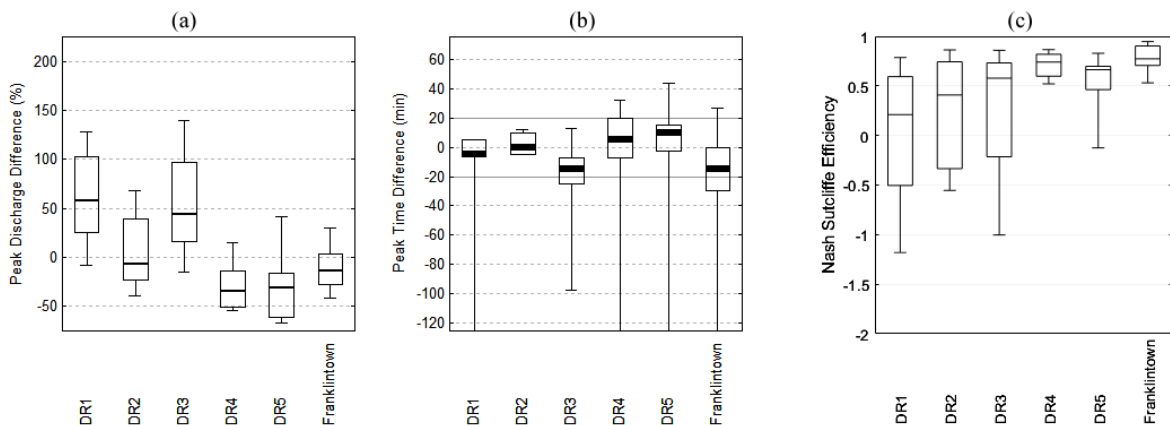
660 Smith, J. A., A. J. Miller, M. L. Baeck, P. A. Nelson, G. T. Fisher, and K. L. Meierdiercks (2005a),
661 Extraordinary Flood Response of a Small Urban Watershed to Short-Duration Convective Rainfall,
662 *Journal of Hydrometeorology*, 6(5), 599-617. doi:10.1175/JHM426.1

663 Smith, J. A., M. L. Baeck, K. L. Meierdiercks, P. A. Nelson, A. J. Miller, and E. J. Holland (2005b),
664 Field studies of the storm event hydrologic response in an urbanizing watershed, *Water Resources*
665 *Research*, 41(10), W10413(10415). doi:10.1029/2004wr003712
666 Smith, J. A., M. L. Baeck, G. Villarini, C. Welty, A. J. Miller, and W. F. Krajewski (2012), Analyses of
667 a long-term, high-resolution radar rainfall data set for the Baltimore metropolitan region, *Water*
668 *Resources Research*, 48(4), 1-14. doi:10.1029/2011wr010641
669 ten Veldhuis, M. C., Z. Zhou, L. Yang, S. Liu, and J. Smith (2018), The role of storm scale, position
670 and movement in controlling urban flood response, *Hydrology and Earth System Sciences*, 22(1), 417-
671 436. 10.5194/hess-22-417-2018
672 Wright, D. B., J. A. Smith, and M. L. Baeck (2014a), Flood frequency analysis using radar rainfall
673 fields and stochastic storm transposition, *Water Resources Research*, 50(2), 1592-1615.
674 doi:10.1002/2013WR014224
675 Wright, D. B., R. Mantilla, and C. D. Peters-Lidard (2017), A remote sensing-based tool for assessing
676 rainfall-driven hazards, *Environmental Modelling & Software*, 90, 34-54.
677 doi:10.1016/j.envsoft.2016.12.006
678 Wright, D. B., G. Yu, and J. F. England (2020), Six decades of rainfall and flood frequency analysis
679 using stochastic storm transposition: Review, progress, and prospects, *Journal of Hydrology*, 585,
680 124816. doi:10.1016/j.jhydrol.2020.124816
681 Wright, D. B., J. A. Smith, G. Villarini, and M. L. Baeck (2012), Hydroclimatology of flash flooding
682 in Atlanta, *Water Resources Research*, 48(4). <https://doi.org/10.1029/2011wr011371>
683 Wright, D. B., J. A. Smith, G. Villarini, and M. L. Baeck (2013), Estimating the frequency of extreme
684 rainfall using weather radar and stochastic storm transposition, *Journal of Hydrology*, 488, 150-165.
685 doi:10.1016/j.jhydrol.2013.03.003
686 Wright, D. B., J. A. Smith, G. Villarini, and M. L. Baeck (2014b), Long-term high-resolution radar
687 rainfall fields for urban hydrology, *Journal of the American Water Resources Association*, 50(3), 713-
688 734. doi:10.1111/jawr.12139
689 Yang, L., J. A. Smith, M. L. Baeck, and Y. Zhang (2016), Flash flooding in small urban watersheds:
690 Storm event hydrologic response, *Water Resources Research*, doi:doi:10.1002/2015WR018326.
691 doi:10.1002/2015WR018326
692 Yang, Y., L. Sun, R. Li, J. Yin, and D. Yu (2020), Linking a Storm Water Management Model to a
693 Novel Two-Dimensional Model for Urban Pluvial Flood Modeling, *International Journal of Disaster*
694 *Risk Science*, 11(4), 508-518. 10.1007/s13753-020-00278-7
695 Yin, J., D. Yu, Z. Yin, M. Liu, and Q. He (2016), Evaluating the impact and risk of pluvial flash flood
696 on intra-urban road network: A case study in the city center of Shanghai, China, *Journal of Hydrology*,
697 537, 138-145. <https://doi.org/10.1016/j.jhydrol.2016.03.037>
698 Yu, G., D. B. Wright, Z. Zhu, C. Smith, and K. D. Holman (2019), Process-based flood frequency
699 analysis in an agricultural watershed exhibiting nonstationary flood seasonality, *Hydrol. Earth Syst.*
700 *Sci.*, 23(5), 2225-2243. doi:10.5194/hess-23-2225-2019
701 Zhou, Z., J. A. Smith, D. B. Wright, M. L. Baeck, and S. Liu (2019), Storm catalog-based analysis of
702 rainfall heterogeneity and frequency in a complex terrain, *Water Resources Research*, 55(3), 1871-
703 1889. doi:10.1029/2018WR023567
704 Zhou, Z., J. A. Smith, L. Yang, M. L. Baeck, M. Chaney, M.-C. Ten Veldhuis, H. Deng, and S. Liu
705 (2017), The complexities of urban flood response: Flood frequency analyses for the Charlotte
706 Metropolitan Region, *Water Resources Research*, 53(8), 7401-7425. doi:10.1002/2016WR019997

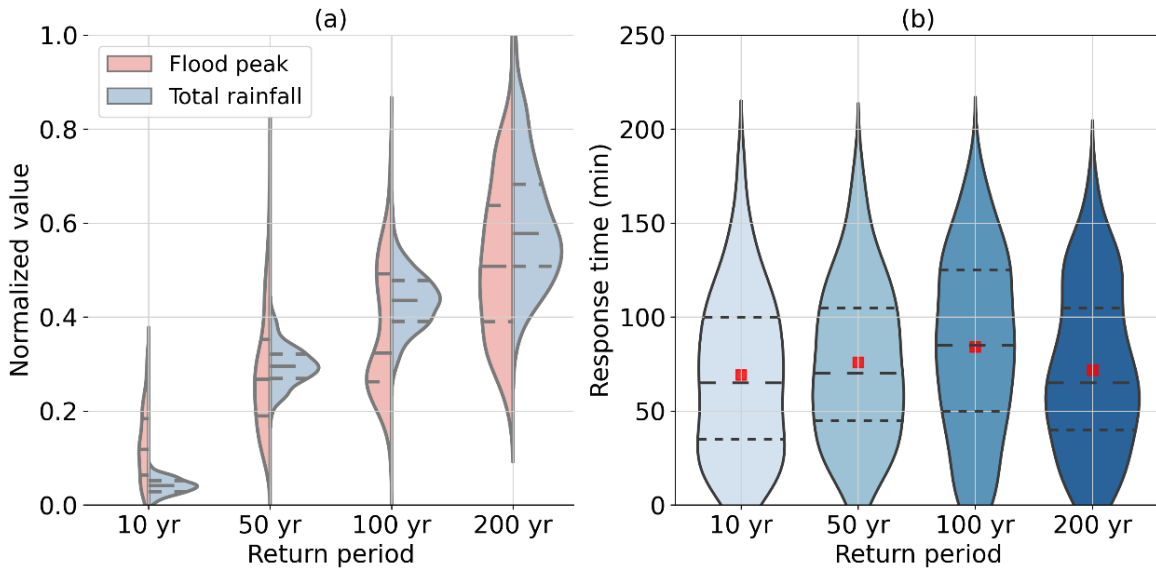
707 Zhu, Z., D. B. Wright, and G. Yu (2018), The Impact of Rainfall Space-Time Structure in Flood
 708 Frequency Analysis, *Water Resources Research*, 54(11), 8983-8998. doi:10.1029/2018wr023550
 709 Zoccatelli, D., M. Borga, A. Viglione, G. B. Chirico, and G. Blöschl (2011), Spatial moments of
 710 catchment rainfall: rainfall spatial organisation, basin morphology, and flood response, *Hydrology and
 711 Earth System Sciences*, 15(12), 3767-3783. 10.5194/hess-15-3767-2011
 712
 713



714
 715 **Figure 1. Overview of Dead Run study region including (a) location of DR, elevation, and transposition**
 716 **domain of SST; (b) land use land cover and stream gages. Land use land cover was obtained from the National**
 717 **Land Cover Data set (NLCD, <http://www.mrlc.gov>)**

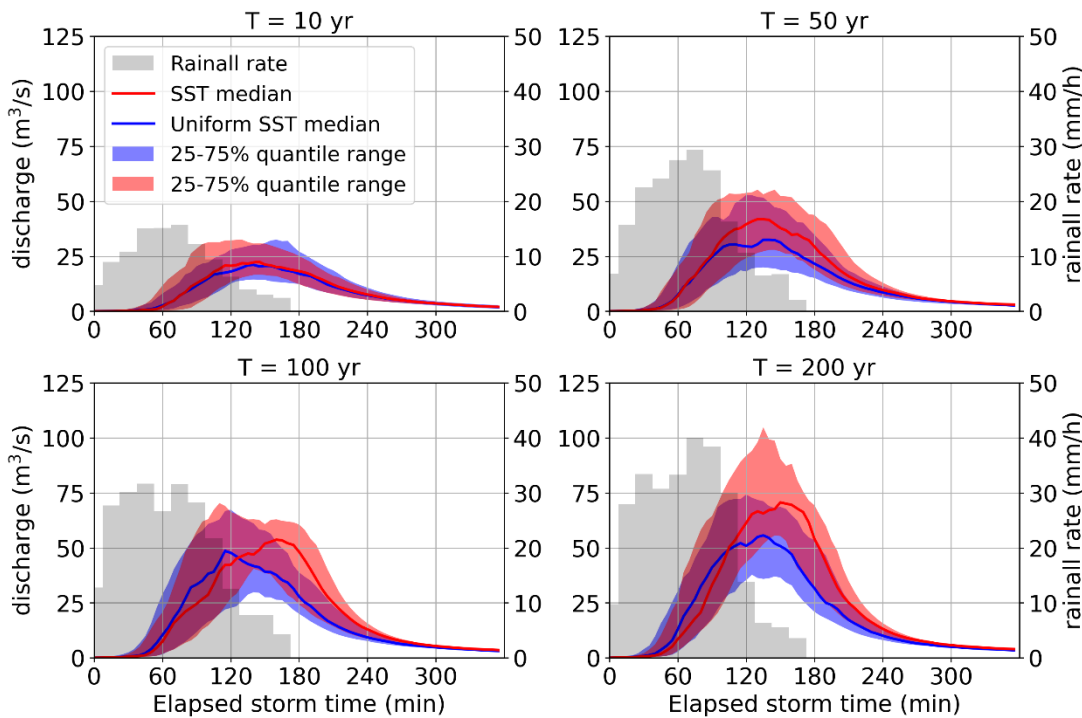


718
 719 **Figure 2. Comparison of (a) flood peak discharges, (b) response times and (c) NSE for 21 historical rainfall events.**
 720



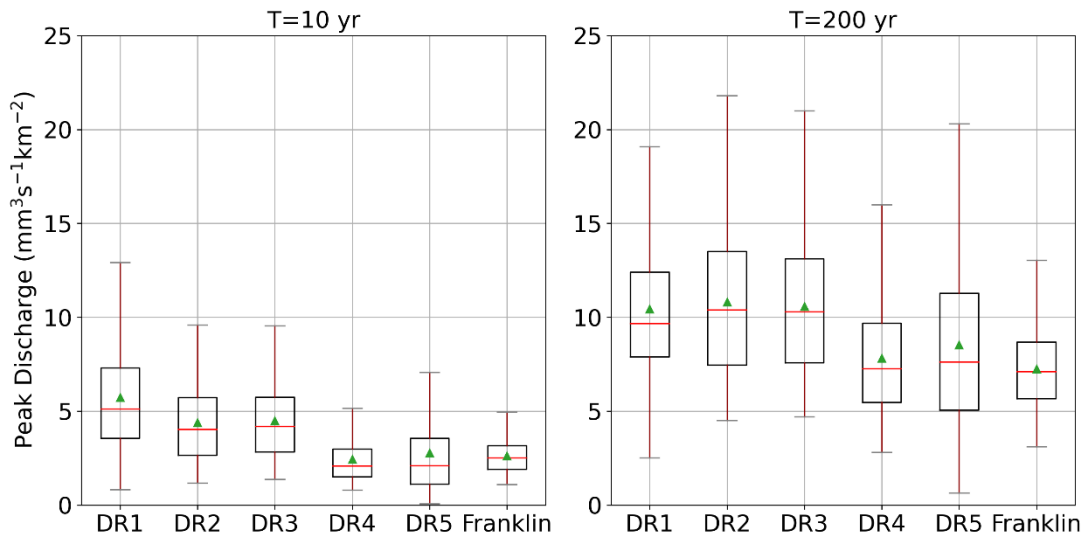
721

722 **Figure 3. Violin plots of (a) normalized flood peak and normalized total rainfall; and (b) response time based on the**
 723 **3-h design storms from 10-y to 200-y return periods. (The red dot indicates mean value. Dashed line in the middle**
 724 **indicates the median value. Upper and lower dashed lines indicate the 75th and 25th quantiles, respectively.)**



725

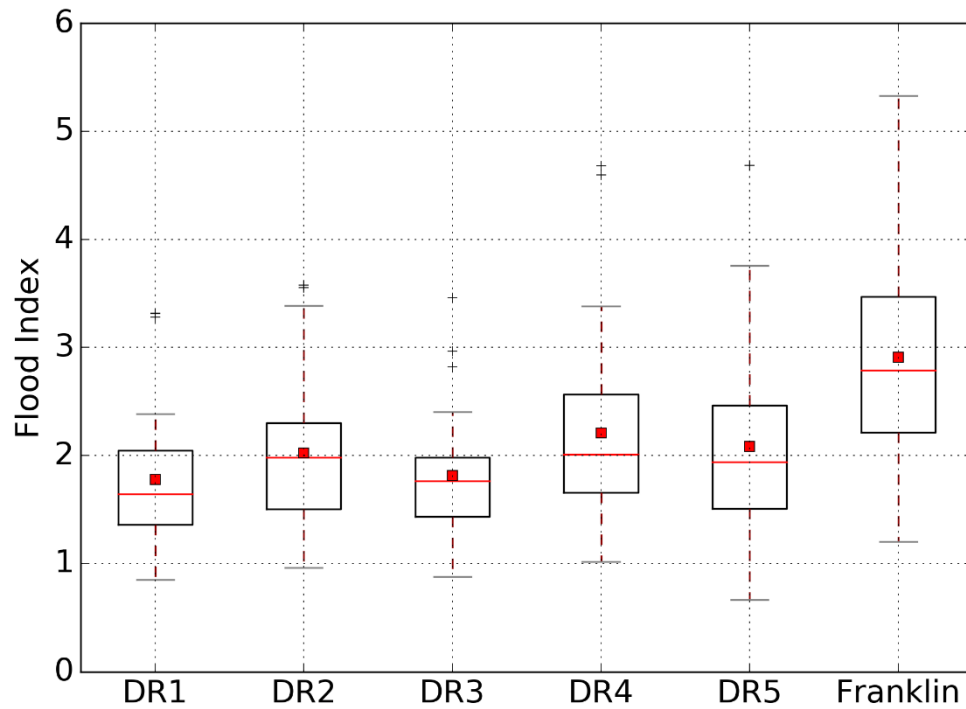
726 **Figure 4. Time series of simulated hydrographs for Franklinton based on the 3-h design storms from 10-yr to 200-**
 727 **yr return periods with spatially uniform (blue) and spatially distributed (red) rainfall. The grey bar indicates the**
 728 **median value of basin-averaged rainfall rate.**



729

730

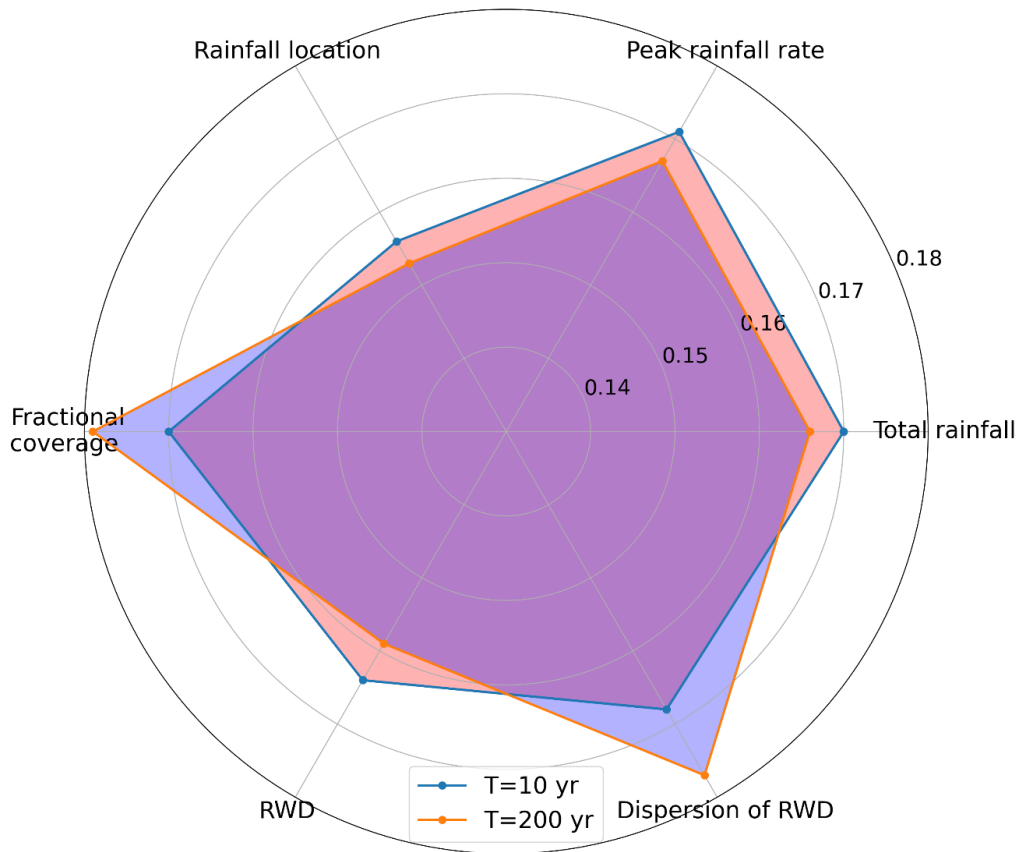
Figure 5. Boxplots of normalized flood peaks for Franklinton and five subwatersheds.



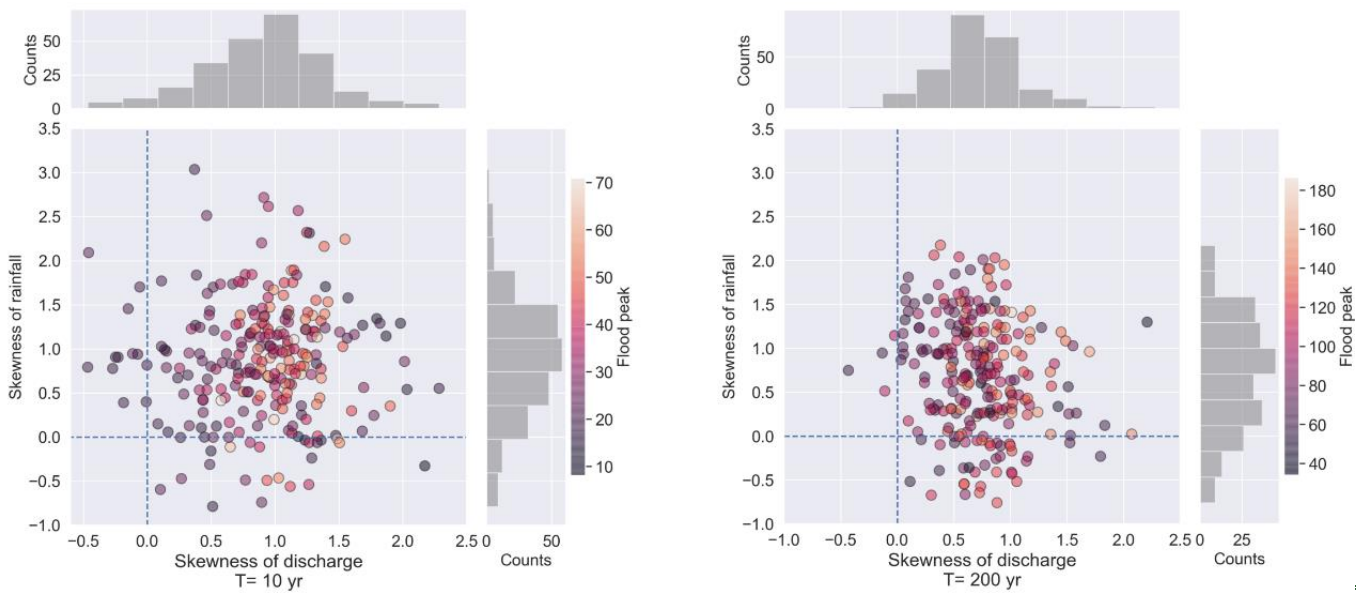
731

732

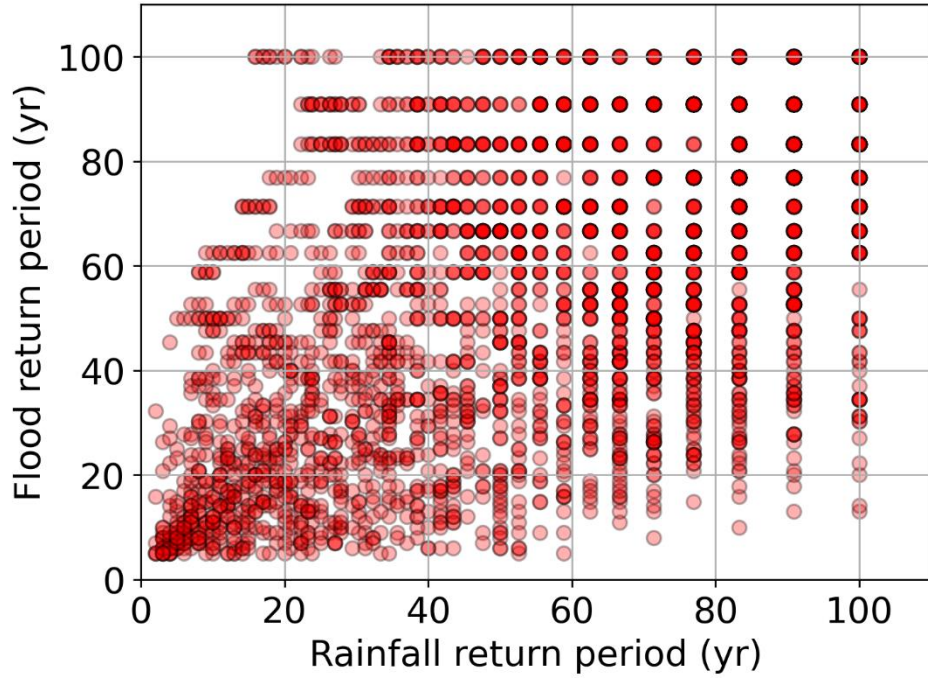
Figure 6. Boxplot of flood index across the DR subwatersheds for the 100-yr design storms.



733
 734 **Figure 7. Feature importance analysis of RF model for space-time rainfall structure and 10-yr (red) and 200-yr (blue)**
 735 **flood peaks.**



736
 737 **Figure 8. Scatter plots of skewness of rainfall and peak discharge — left: 10-yr return period; right: 200-yr return**
 738 **period.**



739

740 **Figure 9. Scatterplot comparison return periods for rainfall and peak discharge for individual SST-based**
 741 **simulations.**

742

743 **Table 1: Characteristics of Dead Run watershed.**

	USGS ID	Area- (km ²)	Developed Land (%)	Imperviousness- (%)	Controlled- area (%)
DR1	01589317	1.32	99%	73.6	41.9
DR2	01589316	1.92	98%	55.5	18.5
DR3	01589320	4.95	98%	62.2	24.4
DR4	01589315	6.29	98%	51.5	12.2
DR5	01589312	2.05	96%	47.9	3.2
Franklinton	01589330	14.3	96%	52.3	25.1

744

Table 2. The median flood peak reductions using spatially uniform and spatially distributed rainfall.

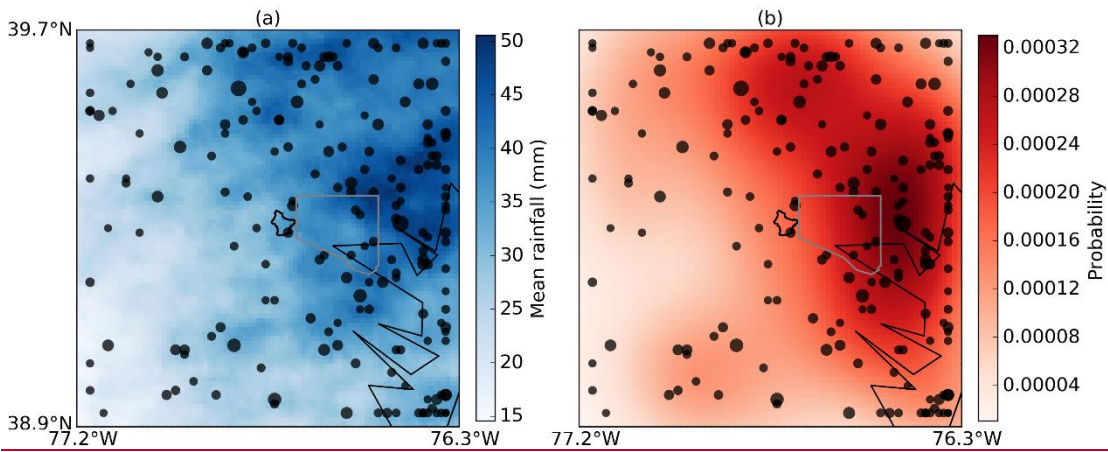
	T=10 yr	T=50 yr	T=100 yr	T=200 yr
DR1	14%	20%	13%	26%
DR2	19%	40%	28%	42%
DR3	24%	33%	27%	31%
DR4	32%	51%	38%	35%
DR5	15%	75%	37%	30%
Franklin	22%	36%	31%	42%

745

746

747

Appendix A

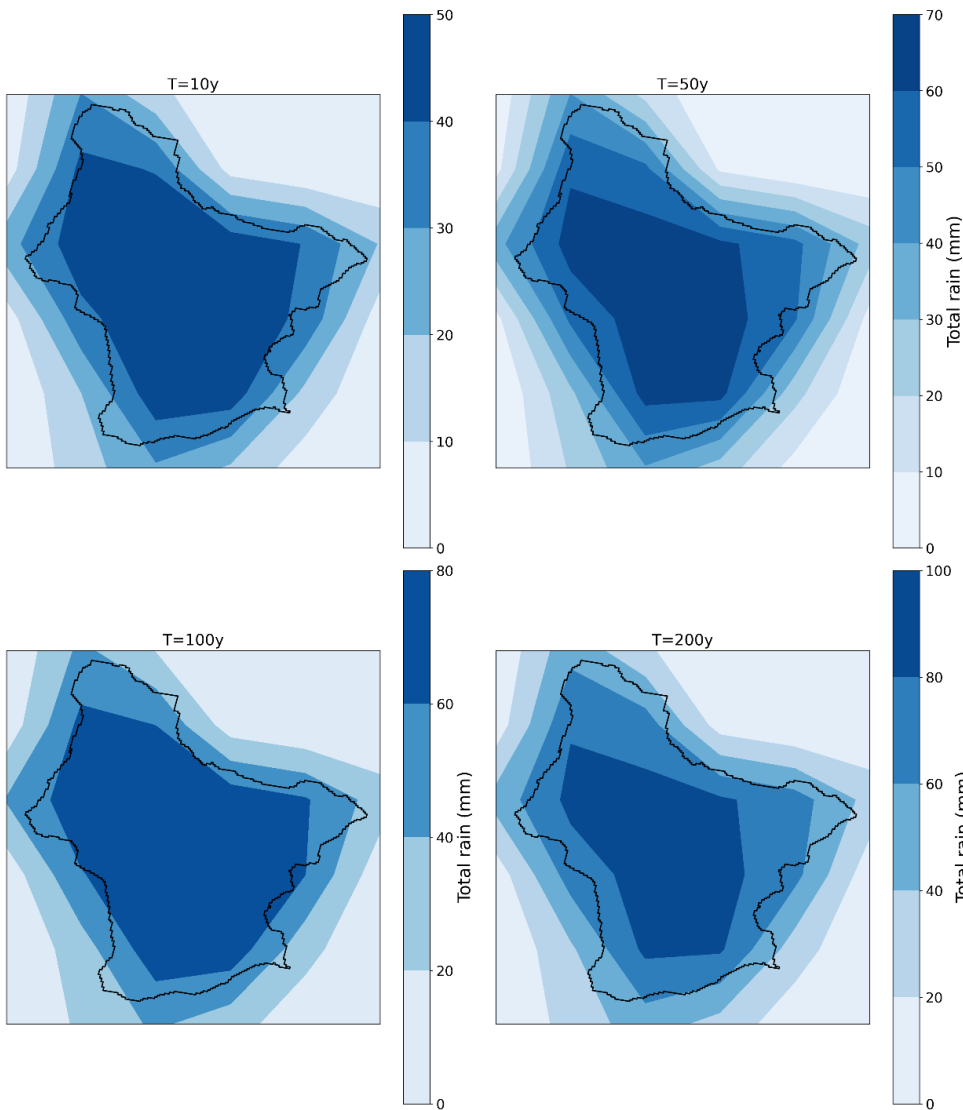


748

749

750

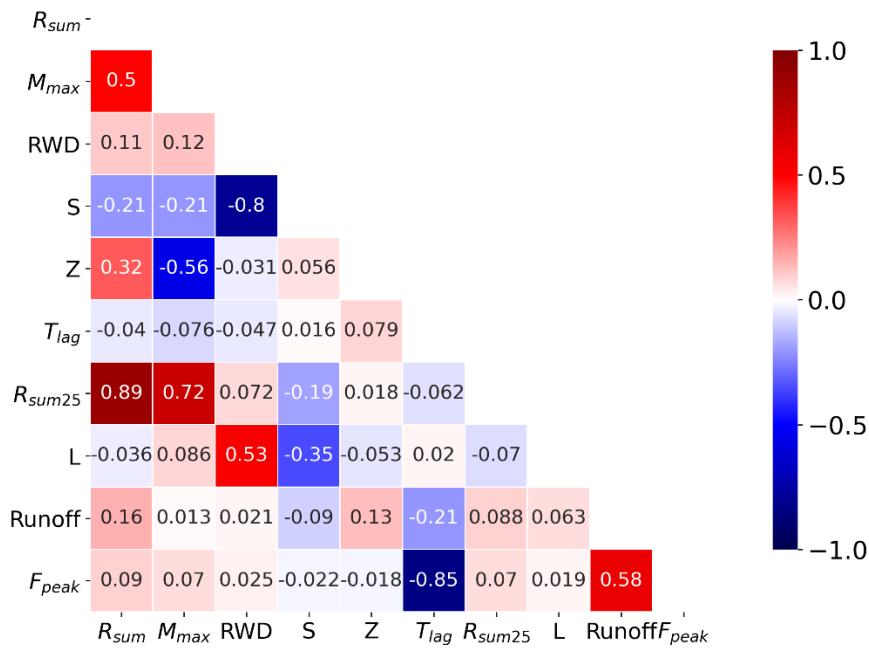
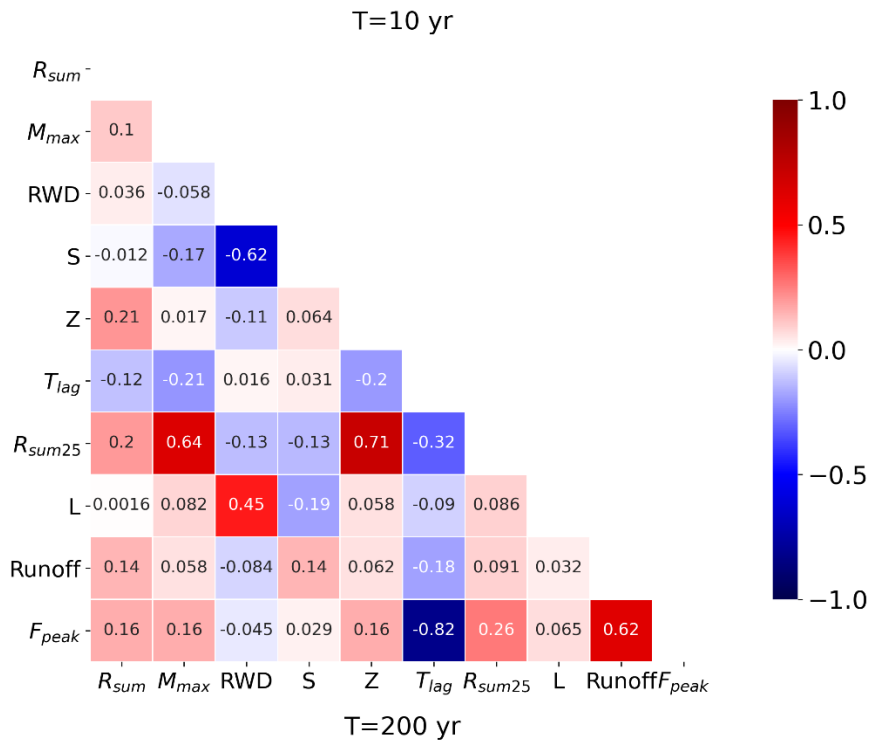
Figure A1: Maps of mean storm total rainfall (a) and probability of storm occurrence (b) for the 200 storms in the 3-h storm catalog (The black dot indicates the location of rainfall centroid).



751

752

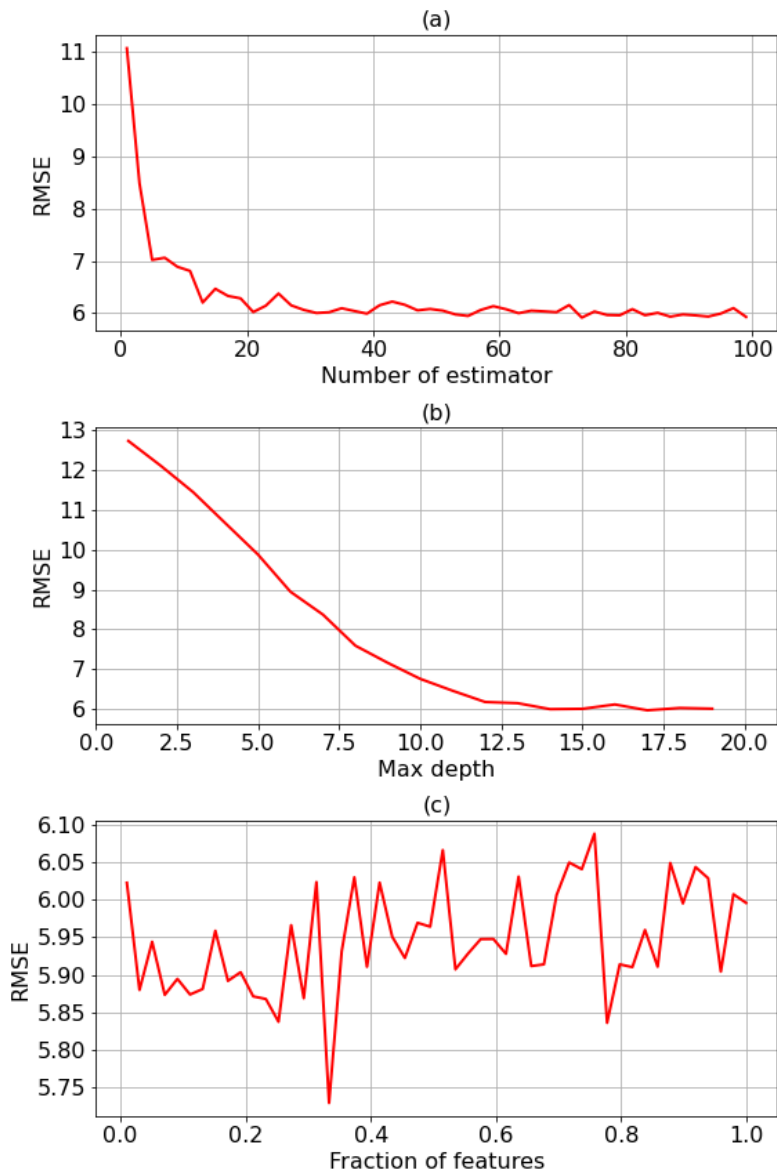
Figure A2: Composite map of rainfall distribution for the 10-y, 50-y, 100-y and 200-y return periods.



753

754 Figure A3: Correlation between space-time rainfall structure and flood responses at Franklinton under 10-yr and 200-yr
 755 return periods.

756



757
 758 Figure A4: The parameter tuning process of RF model (use RMSE for example)
 759